Πανεπιστημιο Κρητης

ΠΜΣ «Οπτικη & Οραση»

Μεταπτυχιακη Εργασια

Επίδραση της ανομοιομορφίας του πλέγματος των φωτοϋποδοχέων στη διακριτική ικανότητα

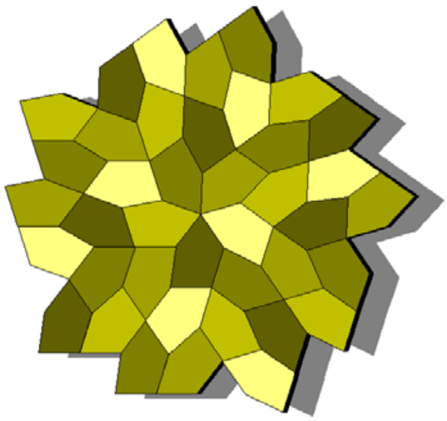

Επιμέλεια: Μ. Θεοδωράκης

Εξεταστική Επιτροπή: **Ι. Παλλήκαρης**
Μ. Τσιλιμπάρης
Χ. Γκίνης

ΕΛΛΑΔΑ 2008
Ανάπτυξη παντού. Ανάπτυξη για όλους.

ΥΠΟΥΡΓΕΙΟ ΕΘΝΙΚΗΣ ΠΑΙΔΕΙΑΣ ΚΑΙ ΘΡΗΣΚΕΥΜΑΤΩΝ
ΕΙΔΙΚΗ ΥΠΗΡΕΣΙΑ ΔΙΑΧΕΙΡΙΣΗΣ ΕΠΕΑΕΚ
ΕΥΡΩΠΑΪΚΗ ΕΝΩΣΗ
ΣΥΓΧΡΗΜΑΤΟΔΟΤΗΣΗ
ΕΥΡΩΠΑΪΚΟ ΚΟΙΝΩΝΙΚΟ ΤΑΜΕΙΟ
ΕΥΡΩΠΑΪΚΟ ΤΑΜΕΙΟ ΠΕΡΙΦΕΡΕΙΑΚΗΣ ΑΝΑΠΤΥΞΗΣ

Η ΠΑΙΔΕΙΑ ΣΤΗΝ ΚΟΡΥΦΗ
Επιχειρησιακό Πρόγραμμα
Εκπαίδευσης και Αρχικής
Επαγγελματικής Κατάρτισης

... Ἀρίσταρχος δὲ ὁ Σάμιος ὑποθέσιών τινῶν ἐξέδωκεν γραφάς, ἐν αἷς ἐκ τῶν ὑποκειμένων συμβαίνει τὸν κόσμον πολλαπλάσιον εἶμεν τοῦ νῦν εἰρημένου. Ὑποτίθεται γὰρ τὰ μὲν ἀπλανέα τῶν ἄστρων καὶ τὸν ἅλιον μένειν ἀκίνητον, τὰν δὲ γᾶν περιφέρεσθαι περὶ τὸν ἅλιον κατὰ κύκλου περιφέρειαν, ὅς ἐστιν ἐν μέσῳ τῷ δρόμῳ κείμενος, τὰν δὲ τῶν ἀπλανέων ἄστρων σφαῖραν περὶ τὸ αὐτὸ κέντρον τῷ ἁλίῳ κειμέναν τῷ μεγέθει τηλικαύταν εἶμεν, ὥστε τὸν κύκλον, καθ᾽ ὃν τὰν γᾶν ὑποτίθεται περιφέρεσθαι, τοιαύταν ἔχειν ἀναλογίαν ποτὶ τὰν τῶν ἀπλανέων ἀποστασίαν, οἵαν ἔχει τὸ κέντρον τᾶς σφαίρας ποτὶ τὰν ἐπιφάνειαν ...

Ἀρχιμήδης, Ψαμμίτης

...Aristarchus of Samos has set forth writings of certain hypotheses, in which from the things that are established it follows that the universe is many times greater than that now told. For it is proposed that the fixed [ones] of the stars and the sun remain motionless, and that the earth is borne around the sun along the circumference of a circle, [the sun] remaining in the middle of the course, and the sphere of the fixed stars lying around the same center as the sun being of so great a magnitude, that the circle, along which the earth is presumed to be borne, has such a proportion to the distance of the fixed [ones], as the center of the sphere has to the surface...

Archimedes, The sand reckoner

Table of Contents

Table of Figures

Περίληψη

Είναι γνωστό ότι η κατανομή και η πυκνότητα της διάταξης των φωτοϋποδοχέων επηρεάζουν τη διακριτική ικανότητα του ανθρώπινου οπτικού συστήματος. Πρωτεύον στόχος της παρούσης βιβλιογραφικής ανασκόπησης είναι να ελεγχθεί αν η ασυμμετρία στο πλέγμα των φωτοϋποδοχέων έχει κάποια επίδραση στη διακριτική ικανότητα.

Προς τούτο, εξετάζονται το αναφερόμενο σχήμα και μέγεθος των κωνίων στην περιοχή της ωχράς, παρακεντρικά και στην περιφέρεια του αμφιβληστροειδή και συγκρίνονται με τη διακριτική ικανότητα που βιβλιογραφικά αποδίδεται σε κάθε περιοχή του αμφιβληστροειδή.

Ειδικά στην περιοχή της ωχράς, η σύγκριση πραγματοποιείται θεωρώντας απόλυτα συμμετρική εξαγωνική την κατανομή των φωτοϋποδοχέων, αλλά και εναλλακτικά μοντέλα κάλυψης της επιφάνειας του αμφιβληστροειδή, που οδηγούν σε περίπου συμμετρικές διατάξεις κωνίων, χωρίς μεταβολή στην μέση χωρική πυκνότητά τους.

Επιβεβαιώνεται ότι παρατηρείται συστηματικά λιγότερο aliasing για υψίσυχνα οπτικά ερεθίσματα από ό,τι θα αναμενόταν, αν αποκλειστικός ρυθμιστικός παράγοντας ήταν η συχνότητα Nyquist της διάταξης των κωνίων.

Στην ωχρά, αν παραβλεφθεί η επίδραση των οπτικών στοιχείων, παρατηρείται aliasing μόλις η χωρική συχνότητα του ερεθίσματος υπερβεί τη συχνότητα Nyquist του πλέγματος των φωτοϋποδοχέων.

Παρακεντρικά, όπου η απόκλιση από τη συμμετρία είναι σημαντική, το όριο Nyquist υπερπηδάται ευκολότερα.

Στην περιφέρεια, δεν παρατηρείται ποτέ aliasing, αλλά αυτό συμβαίνει εξαιτίας της πολύ αραιής διάταξης κωνίων, της μεγάλης αύξησης του μεγέθους των υποδεκτικών πεδίων και της νευρωνικής υποδειγματοληψίας..

Άρα, διαφαίνεται ότι η ασυμμετρία στη διάταξη των κωνίων είναι καθοριστικός παράγοντας για την ανίχνευση και κατανόηση ερεθισμάτων, των οποίων η χωρική συχνότητα υπερβαίνει το όριο Nyquist, όπως είναι οι οφθαλμικές κινήσεις και η ανώτερη επεξεργασία στον οπτικό φλοιό.

Επιπλέον έρευνα για τον καθορισμό της ακριβούς επίδρασής της θα πρέπει να περιλαμβάνει τη μελέτη εναλλακτικών δομών ασύμμετρης διάταξης των φωτοϋποδοχέων, την εφαρμογή τεχνικών τυφλής αποσυνέλιξης σε πραγματικό χρόνο, αλλά και την αξιολόγηση με φυσικές εικόνες, των οποίων το φάσμα ισχύος αποδίδεται αποτελεσματικότερα σε ασύμμετρες κατανομές κωνίων.

Abstract

The effect of asymmetry in the photoreceptor mosaic on visual resolution

It is known that the packing geometry and density of photoreceptors have an effect on the spatial resolution of the human visual system. The primary objective of this work is to evaluate the effects of deviations in the spatial symmetry of the photoreceptor mosaic on spatial resolution.

To this end, the reported shape and spacing of cone photoreceptors are examined in the foveal, parafoveal and peripheral retina and compared against the normally perceived spatial resolution.

Especially in the fovea, this is done assuming a symmetrical hexagonal photoreceptor mosaic and alternative models of retina tiling that result in quasi-symmetrical patterns of photoreceptors, without change in the mean cone density.

It is verified that there is uniformly less aliasing reported for high spatial frequency stimuli, than would be expected if the sole limitation were the cone Nyquist frequency.

In the fovea, when the optics as a limiting factor is bypassed, aliasing is produced only slightly above the Nyquist limit.

Parafoveally, where the departure from symmetry is significant, the cone Nyquist limit is more easily overcome.

In the periphery, aliasing never appears, but this is due to the scarcity of cones and great increase in receptive field size and neural undersampling.

Therefore, it is assumed that the asymmetry in cone packing is a significant factor in detecting and understanding stimuli exceeding the Nyquist limit, along with ocular movements and higher processing in the visual cortex.

Research that would help elucidate its exact effect should encompass alternative asymmetrical models of retina tiling, the effective application of blind deconvolution techniques in real time experiments and the evaluation of natural imagery, whose power spectrum seems to be more efficiently rendered on asymmetrical mosaics.

Chapter 1: The human visual system

The human visual system resembles that of most vertebrates. A brief description of its components follows, starting from its most quintessential component, the eye, and continuing serially towards the visual cortex.

The eye

Looking into the eye, several structures are easily identifiable:

A black-looking aperture, the pupil, that allows light to enter the eye (it appears dark because of the absorbing pigments in the retina).

A colored circular muscle, the iris, which is pigmented (the central aperture of the iris is the pupil). This circular muscle controls the size of the pupil so that more or less light, depending on conditions, is allowed to enter the eye. Eye color, or more correctly, iris color is due to variable amounts of eumelanin (brown/black melanins) and pheomelanin (red/yellow melanins) produced by melanocytes. More of the former is in brown eyed people and of the latter in blue and green-eyed people.

A transparent external surface, the cornea, that covers both the pupil and the iris. This is the first and most powerful lens of the optical system of the eye and allows, together with the crystalline lens the production of a sharp image at the retinal photoreceptor level.

The "white of the eye", the sclera, which forms part of the supporting wall of the eyeball. The sclera is continuous with the cornea. Furthermore this external covering of the eye is in continuity with the dura of the central nervous system.

When the eye globe is removed from the orbit, we can see that the eye is a slightly asymmetrical sphere with an approximate sagittal diameter or length of 24 to 25 mm. and a transverse diameter of 24 mm. It has a volume of about 6.5 cc.

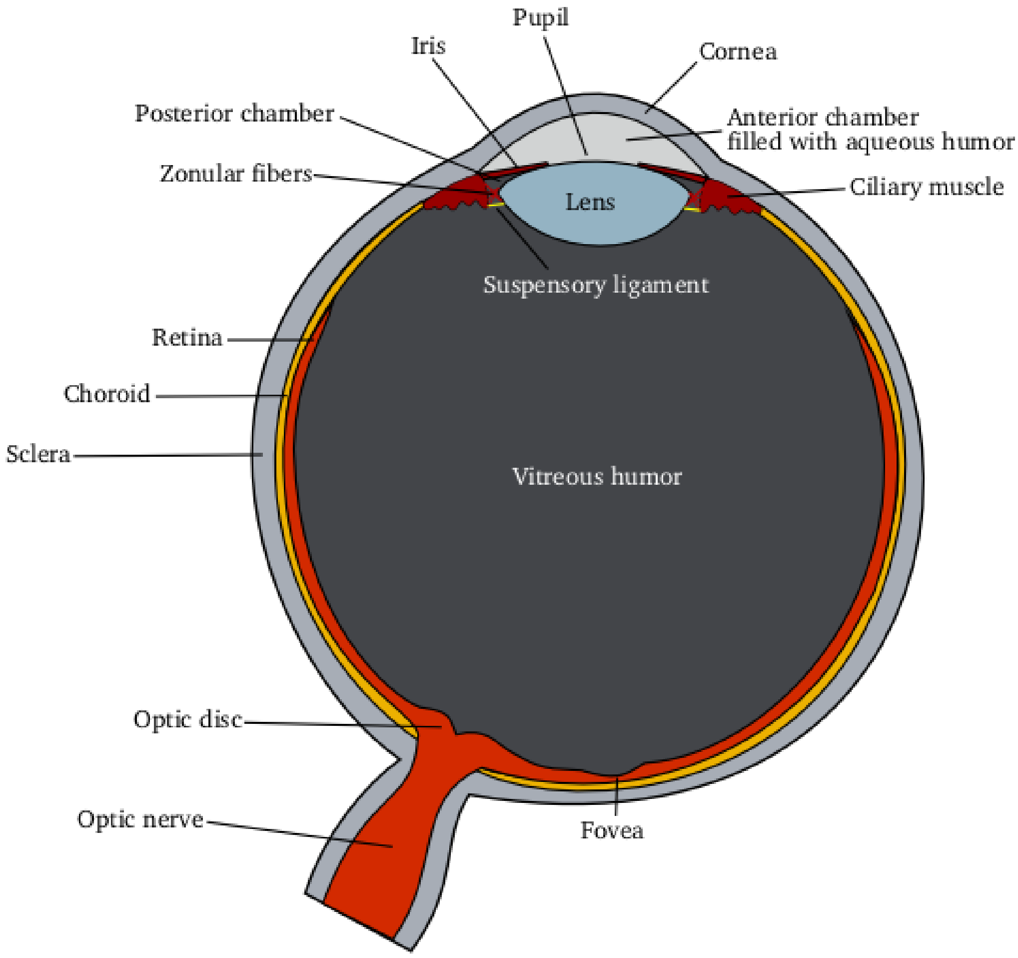

Figure 1: Sagital section of the adult human eye (PD)

A cross-sectional view of the eye shows three different layers:

1. The external layer, formed by the sclera and cornea

2. The intermediate layer, divided into two parts: anterior (iris and ciliary body) and posterior (choroid)

3. The internal layer, or the sensory part of the eye, the retina

Additionally, three chambers of fluid are apparent: the Anterior chamber (between cornea and iris), Posterior chamber (between iris, zonule fibers and lens) and the Vitreous chamber (between the lens and the retina). The first two chambers are filled with aqueous humor whereas the vitreous chamber is filled with a more viscous fluid, the vitreous humor.

The sagittal section of the eye also reveals the lens which is a transparent body located behind the iris. The lens is suspended by ligaments (called zonule fibers) attached to the anterior portion of the ciliary body. The contraction or relaxation of these ligaments as a consequence of ciliary muscle actions, changes the shape of the lens, a process called accommodation that allows us to form a sharp image on the retina.

Light rays are focussed through the transparent cornea and lens upon the retina. The central point for image focus (the visual axis) in the human retina is the fovea. Here a maximally focussed image initiates resolution of the finest detail and direct transmission of that detail to the brain for the higher operations needed for perception. Slightly more nasally than the visual axis is the optic axis projecting closer to the optic nerve head. The optic axis is the longest sagittal distance between the front or vertex of the corna and the furthest posterior part of the eyeball. It is about the optic axis that the eye is rotated by the eye muscles. Some vertebrate retinas have instead of a fovea, another specialization of the central retina, known as an area centralis or a visual streak.

The retina

An ophthalmocopic view of the retina reveals an image, where its prominent features are easily distinguished.

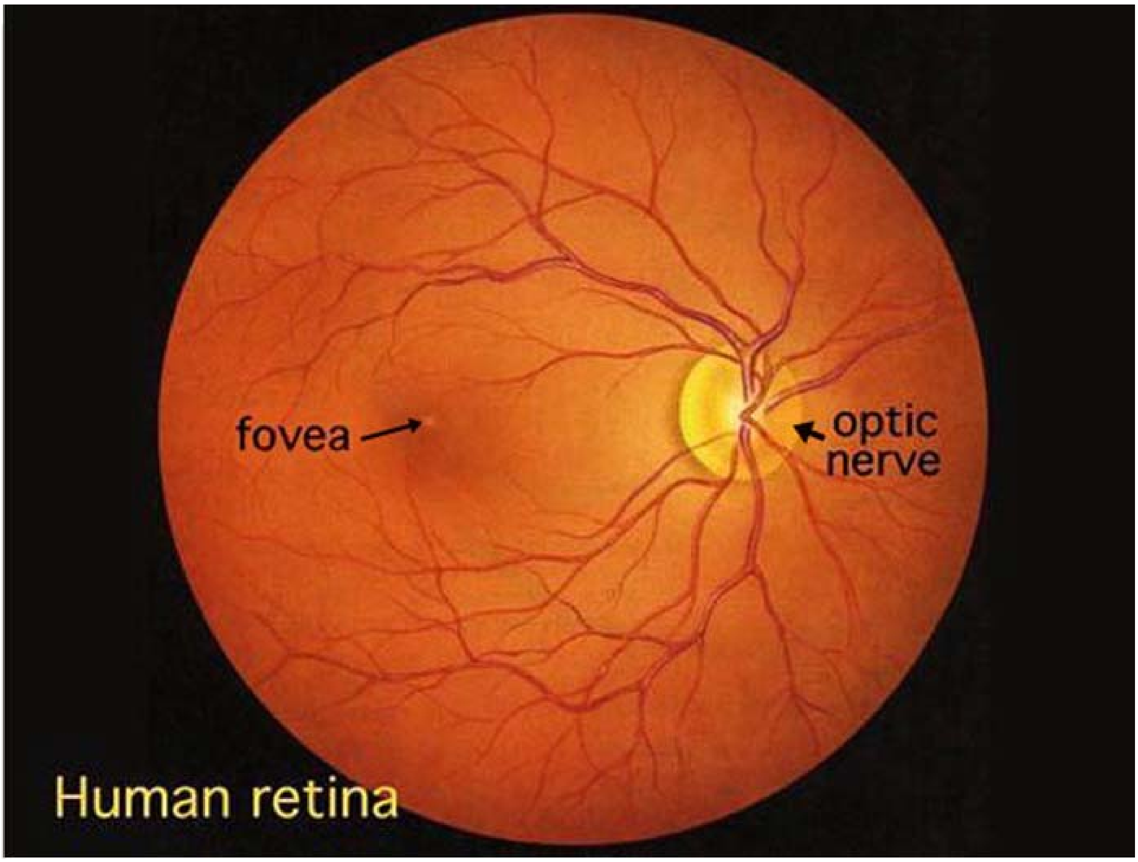

Figure 2: The human retina as seen through an ophthalmoscope (PD)

In the center of the retina is the optic nerve, a circular to oval white area measuring about 2 x 1.5 mm across. From the center of the optic nerve, the major blood vessels of the retina radiate outward. Approximately 17 degrees (4.5-5 mm), or two and half disc diameters to the left of the disc, the slightly oval-shaped, blood vessel-free reddish spot, the fovea can be observed, lying at the center of the area known as the macula.

A circular field of approximately 6 mm around the fovea is considered the central retina while beyond this is peripheral retina stretching to the ora serrata, 21 mm from the center of the optic disc. The total retina is a circular disc of approximately 42 mm diameter.

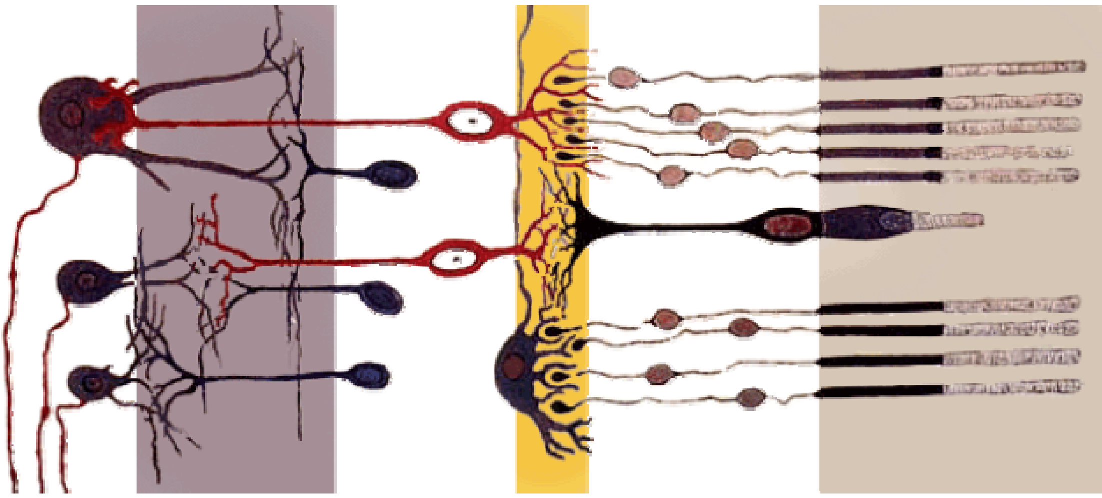

Figure 3: The human retina's axial organisation (PD)

The optic nerve contains the ganglion cell axons running to the brain and, additionally, incoming blood vessels that open into the retina to vascularize the retinal layers and neurons. A radial section of a portion of the retina reveals that the ganglion cells (the output neurons of the retina) lie innermost in the retina closest to the lens and front of the eye, and the photoreceptors (the rods and cones) lie outermost in the retina against the pigment epithelium and choroid. Light must, therefore, travel through the thickness of the retina before striking and activating the rods and cones. Subsequently, the absorbtion of photons by the visual pigment of the photoreceptors is translated into first a biochemical message and then an electrical message that can stimulate all the succeeding neurons of the retina.

The retina is a stack of several neuronal layers. Light is concentrated from the eye and passes across these layers (from left to right) to hit the photoreceptors (right layer). This elicits a chemical transformation mediating a propagation of signals to the bipolar and horizontal cells (middle yellow layer). The signal is then propagated to the amacrine and ganglion cells. These neurons ultimately may produce action potentials on their axons. This spatiotemporal pattern of spikes determines the raw input from the eyes to the brain.

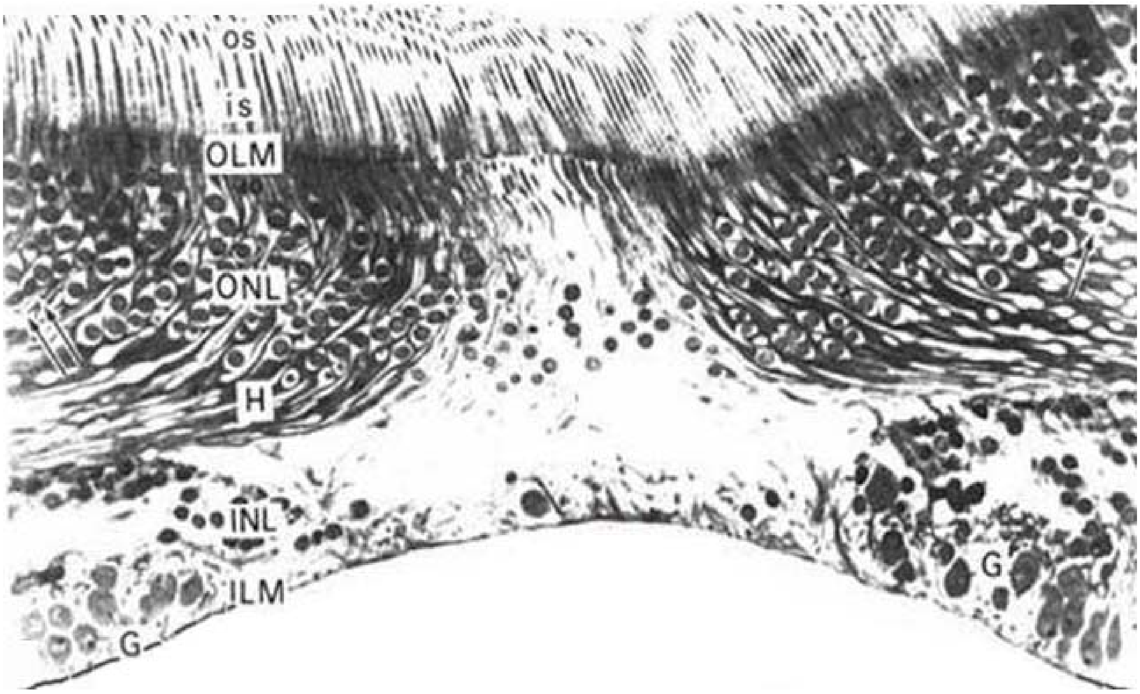

Figure 4: Radial section of the human foveal pit (Yamada, 1969)

The center of the fovea is known as the foveal pit (Polyak, 1941) and is a highly specialized region of the retina different from the central and peripheral retina we have considered so far. A Radial section of this small circular region of retina measuring less than a quarter of a millimeter (200 microns) across is shown above from a human eye, in an image taken from a now famous paper by Yamada.

The photoreceptors – cones in detail

Two or three types of cone photoreceptor and a single type of rod photoreceptor are present in the normal mammalian retina. Some non-mammalian retinas have even more cone types. However, the human retina, which is of particular importance in our study, is populated by three types of cones, often described as S, M and L cones, referring to short, medium and long wavelength.

Rods are much more abundant in total, despite the fact that they are conspicuously absent from the foveal pit. The distribution of all photoreceptors throughout the retina can be observed below.

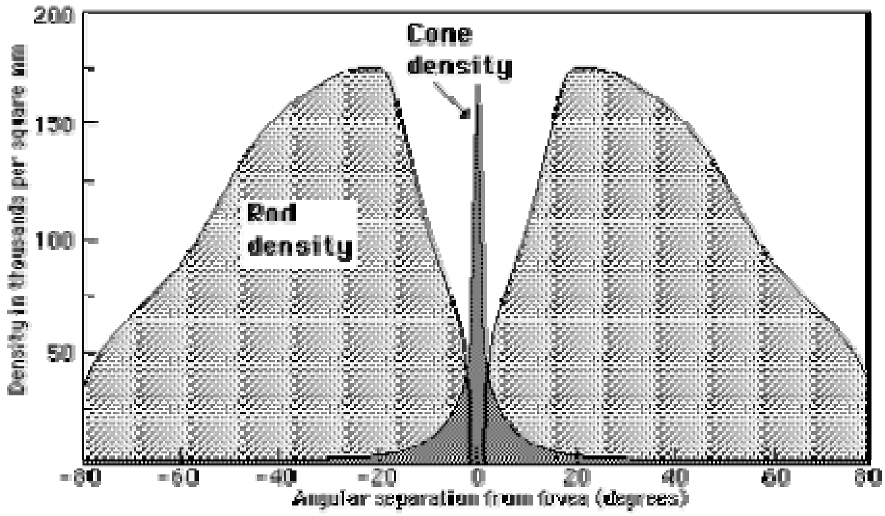

Figure 5: Angular distribution of photoreceptors throughout the retina (PD, replotted)

Cones are robust conical-shaped structures that have their cell bodies situated in a single row right below the outer limiting membrane (OLM) and their inner and outer segments protruding into the subretinal space towards the pigment epithelium. In the foveal retina, where only cones are concentrated, their cell bodies are layered in oblique columns below the outer limiting membrane. Rods, on the other hand, are slim rod-shaped structures with their inner and outer segments filling the area between the larger cones in the subretinal space and stretching to the pigment epithelium cells. Rod cell bodies make up the remainder of the outer nuclear layer below the cone cell bodies. Apical processes from the pigment epithelium envelope the outer segments of both rods and cones (not always clear in histological sections).

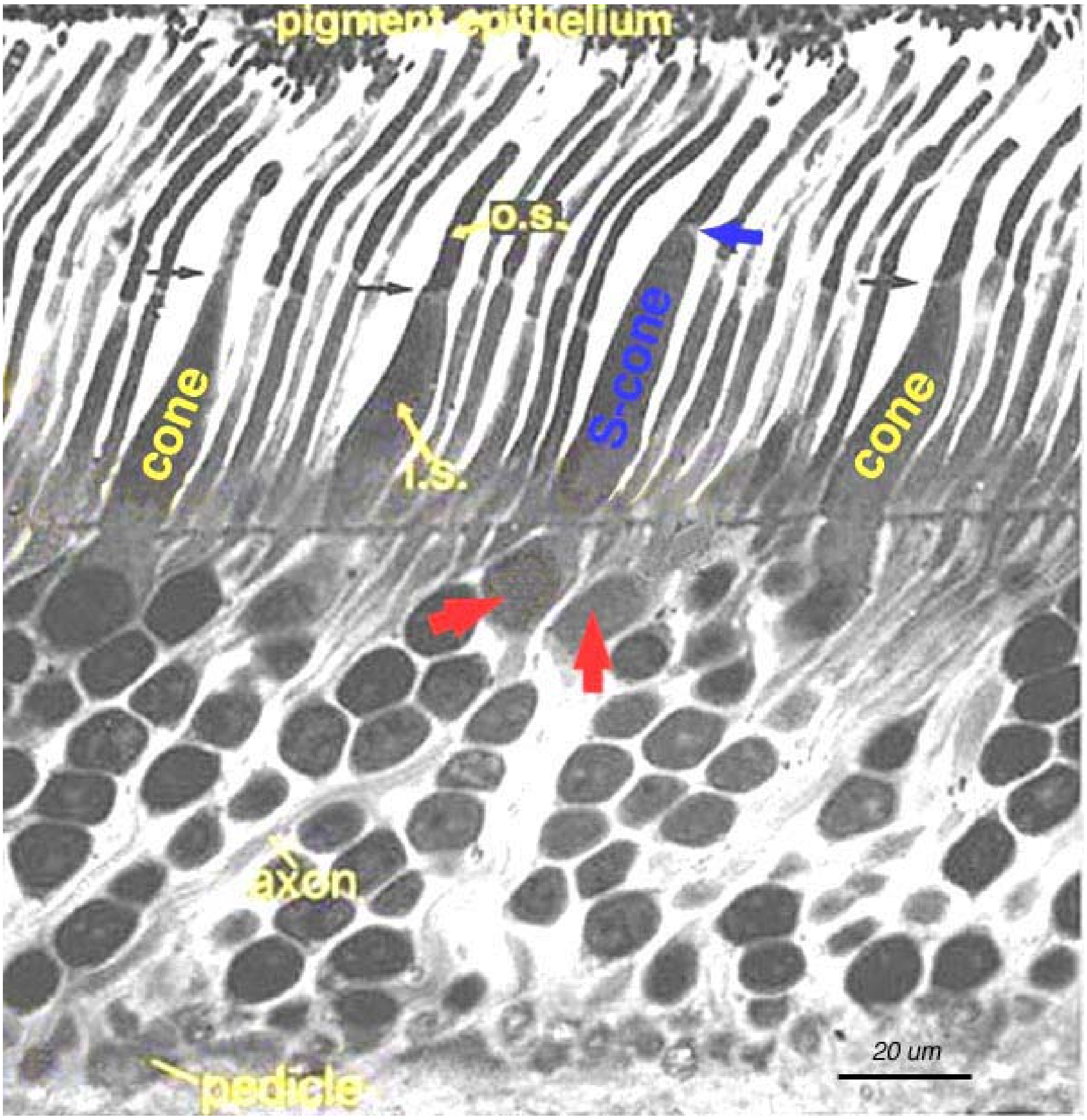

Figure 6: Sagital section of the outer human retina, demonstrating photoreceptors

The photoreceptor consists of 1) an outer segment, filled with stacks of membranes containing the visual pigment molecules such as rhodopsins, 2) an inner segment containing mitochondria, ribosomes and membranes where opsin molecules are assembled and passed to be part of the outer segment discs, 3) a cell body containing the nucleus of the photoreceptor cell and 4) a synaptic terminal where neurotransmission to second order neurons occurs.

Outer and inner segments of rods are generally thinner than those of cones. For example, the rod inner segments are 2 microns and the cone's about 6 microns in diameter in the peripheral human retina. In the fovea, however, where there are only cone photoreceptors, the most central cones are even thinner than the average rod at about 1.5 microns diameter. Inner segment regions of both rods and cones are filled with long thin mitochondria. At the top of the inner segment a thin cilium joins the inner and outer segments of the rods and cones.

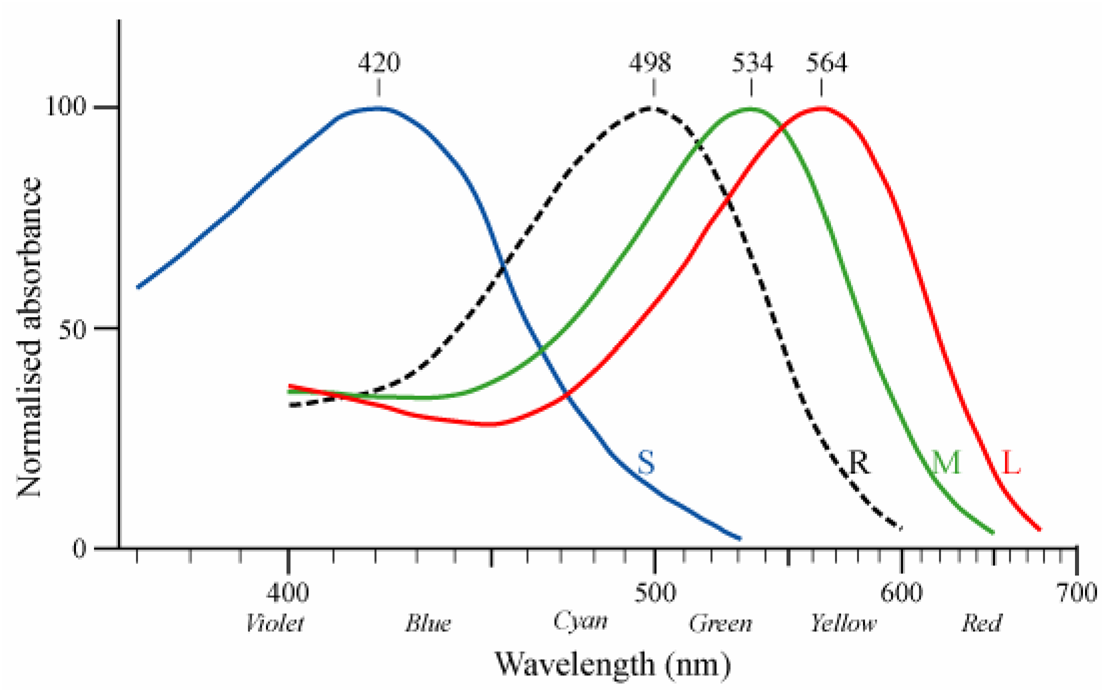

Figure 7: Normalised absorbance of all photoreceptors (S,M,L cones and rods) (Bowmaker, 1980)

Because most people feel more comfortable referring to them by color, rather than by wavelength, they are sometimes called red, green, and blue cones, even though the longest wavelength cone response is actually in the yellow region of the spectrum, short of red. The response of each cone type depends on both the wavelength of light and its amount, or intensity.

Because of this dual dependency, there is an ambiguity in the meaning of the response of any individual photoreceptor. In fact, the magnitude of the response alone cannot tell us anything about the color of the light. For example, if a single long-wavelength photoreceptor gives a particular magnitude response to a given amount of red light (say, 100 photons of wavelength 65o nm), it would give twice as large a response to twice as bright a red light. But a still larger response would be elicited by a mere 100 photons of orange (625 nm) light, because the longwavelength cone responds better to orange light than to red.

Given this ambiguity, and given the broad spectral sensitivity of each of our cones, how can it be that we can distinguish millions of colors? Furthermore, unlike some fish, we do not have any cones that peak in red light, so how can we possibly distinguish red? The answer to both these questions is that the visual system compares the activation of each type of cone with the others. If part of the retina is stimulated by red light, even though the red cones covering that part of the retina would be more effectively activated by shorter wavelength light, the red cones nevertheless will be activated more than the green cones. If the amount of red light increases, increasing the response from both cones, the red cone signal will still be bigger than the green signal. Thus the ratio between the red and green cone responses gives an unambiguous code for the wavelength of light in the yellow-to-red range of the spectrum.

Chapter 2: Measurement of light and visual function

Measurement of light

Light can be measured and specified in two types of units: radiometric units and photometric units. We consider 'light' to be a form of visible electromagnetic radiation. It is part of the electromagnetic spectrum between the wavelengths of 380 nm (blue light) and 750 nm (red light).

Radiometry

There are two parallel sets of units for measuring light. One is based on the psychophysical impact of the light on a human observer, the other on detection by physical radiometric devices. The two units are interconvertible, but sometimes only with difficulty. Measurement of light energy from a source can be specified in radiometric units. Radiometric units specify the amount of radiant energy present in light.

All light measurement is derived from radiant flux. Subsequently, radiometric units are defined with respect to direction and surface, and all photometric units are derived from radiometric units using the photopic luminous efficiency functions or the scotopic luminous efficiency function.

There are two main ways in which energy produces photons, incandescent and luminescent. These correspond to thermal and non-thermal mechanisms, respectively. With incandescence, photons are released from thermally agitated electrons. The frequency of photons from this type of radiation is relatively wide and continuous regardless of the substance, with a spectrum dependent only on temperature. Luminescence involves electron excitation in an atom, molecule or crystal. Emission of photons results from the energy given up by the electron as it moves from one excitation shell to another. The frequency of the photon emission has a pattern characteristic of the substance.

Luminescent production of photons can be achieved in a gas discharge tube. These tubes contain gas vapour such as sodium, mercury or neon. Electrons are accelerated from one electrode to the other in these tubes. These high velocity electrons bombard the gas atoms and causes a displacement of electrons. When the electrons return to the normal state, this excitation energy is emitted as photons. Neon and mercury sources are often used in optics.

Fluorescence is another example of luminescence. In fluorescent tubes, electrons collide with atoms of mercury, resulting in a quanta of ultraviolet light being emitted. Part of the energy of the ultraviolet quanta is absorbed by the phosphor coating of the tube and subsequently releases a quanta of light in the visible spectrum.

A tungsten filament lamp is an example of incandescence. Tungsten spectral emission resembles that of a black body. A black body is a theoretically perfect radiator. As the energy is increased, the spectral emission changes. Colour temperature is a term used when the colour of the radiator is the same colour as the black body at a certain temperature (measured in Kelvin). For example, a black body with a temperature of 2700K would have a similar colour to tungsten, therefore, tungsten is said to have a colour temperature of 2700K.

Photometry

Photometry is the measurement and specification of light relating to its effect on vision. The eye can be regarded as a radiant energy detector with a selective spectral response. In a well lit environment it is maximally sensitive to light of about 555 nm (yellow-green light) and relatively insensitive to far red and blue light. The function describing the response of the human eye to different wavelengths is known as the relative luminous efficiency function.

Measurement of light from a source can be specified in photometric units. Photometric units take into account both the quantity of radiant energy and sensitivity of the eye, to the wavelength(s) of the radiation. In other words, the photometric quantities specify the capacity of radiant energy to evoke a visual response.

All light measurement is derived from radiant flux, converted to luminous flux. As with radiometric units, subsequent photometric units are also defined with respect to direction and surface.

Psychophysical measurements

Psychophysical methods and procedures are useful in determining threshold, including visual field analysis. For a perfect observer, threshold is the point where the stimulus can just be detected or where you just cannot detect the stimulus. Humans are not perfect observers, and often thresholds are defined in probabilistic terms: for example, half the points presented would be detected and half would not. So under certain psychophysical techniques, threshold can be considered the point where 50% of the stimuli are detected. Threshold variability most likely depends on neural noise. One aspect of visual psychophysics deals with noise and is termed, Signal Detection Theory, but this will not be covered here.

Measurement of visual response can be achieved through several methods. These methods include the, 1) Method of Adjustment, 2) Method of Limits, 3) Staircase (modified Method of limits) and 4) Method of Constant Stimuli.

The method of adjustment involves asking the subject to either increase the stimulus intensity from non-seeing until the stimulus can just be seen or to decrease the stimulus intensity until the stimulus has just disappeared. This method also suffers from both errors of habituation and anticipation (these two errors are discussed below) but is useful to obtain an estimate of threshold that can be investigated with more complex techniques.

Stimulus Intensity	A	D	A	D	A	D	A	D
9		Y						
8		Y				Y		Y
7		Y		Y		Y		Y
6		Y		Y		Y		Y
5		Y		Y		Y		Y
4	Y	Y		Y		Y		Y
3	N	Y	Y	Y	Y	Y		Y
2	N	N	N	Y	N	N	Y	Y
1	N	N	N	N	N		N	N
0	N		N		N		N	
-1	N		N		N		N	
-2	N		N		N		N	
-3	N		N		N		N	
-4	N		N		N		N	
-5	N		N				N	
-6	N						N	
Transition Points	3.5	2.5	2.5	1.5	2.5	2.5	1.5	1.5

Mean Threshold = 2.25

Figure 8: Threshold determination using the method of limits (Kalloniatis)

Ascending and descending limits is a quick method of determining threshold, however, like the method of adjustment, two errors can occur; the errors of habituation and the errors of anticipation. The error of habituation occur when subjects develop a habit of responding to a stimulus. For example, in ascending limits, the subject may respond to seeing the stimulus three steps past the threshold every time, thus giving a false threshold point. The error of anticipation occurs when subjects prematurely report seeing the stimulus before the threshold has been reached. Clear instructions, demonstrations and practice runs can reduce the errors of habituation. Errors of anticipation can be minimised by changing the starting intensity for each trial.

A variation of the method of limits is the staircase method which involves both the ascending and descending limits in a trial. Stimulus intensity is progressively increased (ascending limits) until the subject reports seeing the stimulus. At this point, the intensity value is recorded and the stimulus intensity is then progressively reduced (descending limits), until the subject reports not seeing the stimulus. Threshold is considered the average of several of these reversal points. See figure 12. Threshold estimates using this methods are also prone to the errors noted above and consequently, multiple simultaneous staircases are used to minimise such errors.

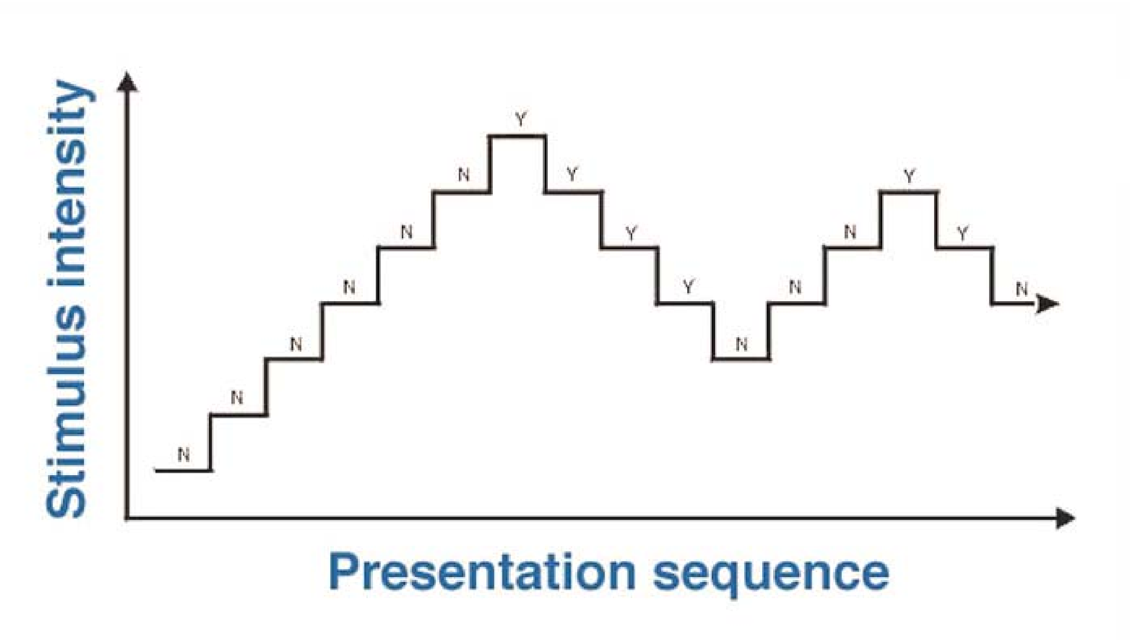

Figure 9: Staircase method (Kalloniatis)

The method of constant stimuli involves the repeated presentation of a number of stimuli. The threshold value of 50% lies somewhere within this range. Other psychophysical techniques are used to estimate threshold and determine stimuli intensities to be used for presentation. These stimuli are randomly presented. The percentage of detection is determined as a function of stimulus intensity. Some high intensity points will always be detected while other low intensity points will never to detected. The percentage of detection versus the stimulus intensity is graphed in Figure 13. This graph is called the psychometric function and looks like an S shaped curve sometimes referred to as an ogive. The threshold value is defined as the value where 50% of the stimuli are detected. Thus the threshold for the data below is 23.5.

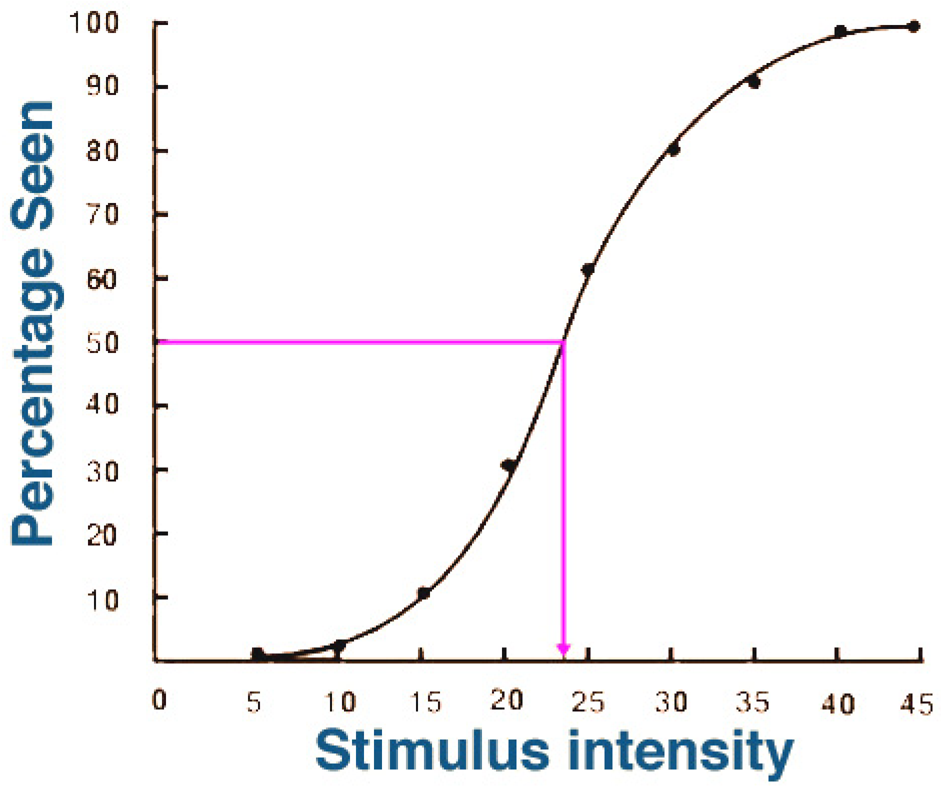

Figure 10: Psychometric function for a YES-NO paradigm (Luu)

Psychophysical procedures are used to minimise the variability in obtaining threshold by requiring subjects to commit to an answer.

The yes-no procedure involves the subject judging the presence or absence of the signal. A stimulus is presented, during which the subject has to make a yes or no response. Correct response can range from 0% to 100% as shown above.

The forced choice procedure involves forcing the subject to choose from alternative choices, one of which contains the stimulus. A two-alternative forced choice (2AFC) describes a subject choosing between two alternatives. Choosing from four alternatives and six alternatives are called 4AFC and 6AFC, respectively. The percentage correct for the various stimuli intensities can be used to construct a psychometric function to determine threshold. As there is already a 50% chance of a correct response with 2AFC, threshold is commonly considered as 75%, which scales down accordingly for more alternatives.

Adaptive psychophysical measurements

Adaptative methods involve presenting signals based on the performance of the subjects previous response while in forced choice tracking a forced choice procedure is used. When subjects correctly respond three times, stimulus intensity is decreased by one step. An incorrect response will result in a one step increase in stimulus intensity. The size of the ascending and descending steps remain the same throughout the session. The session ends when a narrow range of stimuli level is reached. Threshold is considered the average of the intensity level within the period of stable tracking.

The size of the steps is an important factor. If the steps are too small, the subject may not be able to discern differences in intensity. Reaching the threshold range with small steps will also be time consuming. Large steps may miss the threshold range altogether, with swings from well above threshold to well below threshold.

Parameter estimation by sequential testing (PEST) was designed to address the problem of step size and starting intensity. PEST techniques begin the session with large steps (large changes in intensity) with the intensity progressively halved until the smallest specified step to determine threshold.PEST is actually a little more complicated than explained here.

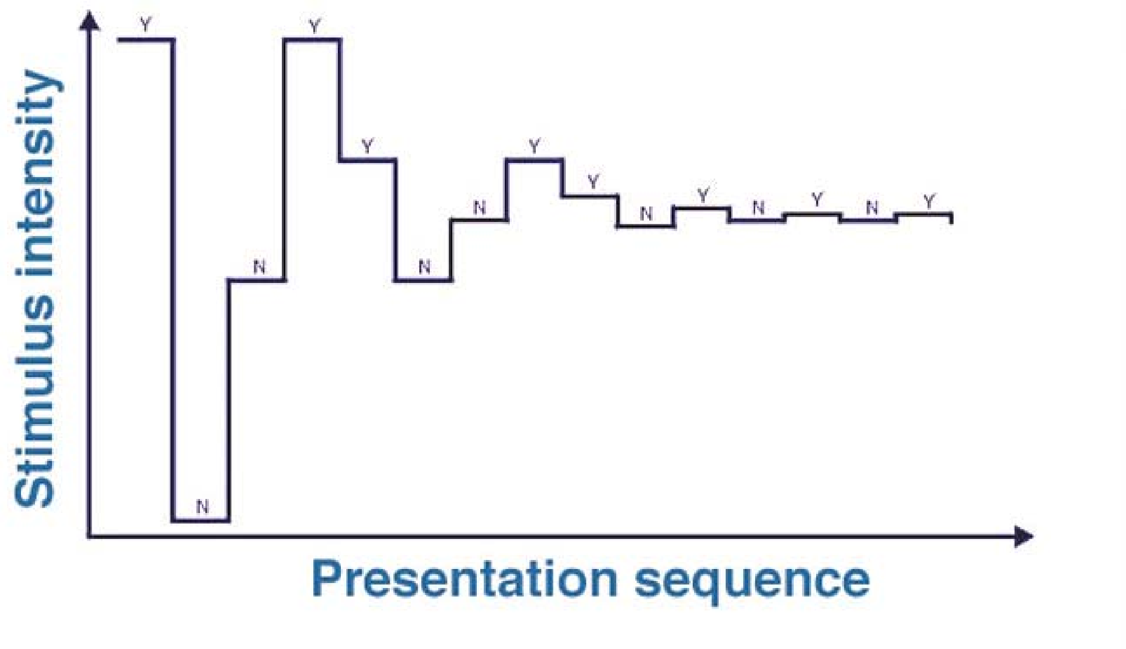

Figure 11: Event tracking using PEST

Maximum likelihood methods. With both forced choice tracking and PEST, subsequent changes in stimulus intensity relies on the subjects previous two or three responses. In maximum likelihood methods, the stimulus intensity presented at each trial is determined by statistical estimation of the subjects threshold based on all responses from the beginning of the session. After each trial, a new estimation of threshold is determined and the stimulus intensity is adjusted accordingly. Threshold is taken at the point where there is little change in stimulus intensity.

Several examples of maximum likelihood methods are QUEST (quick estimate by sequential testing), ZEST (zippy estimate of sequential testing), and SITA (Swedish interactive threshold algorithm - which is a modified ZEST). These methods require prior information about the population's distribution of threshold and is used to construct a probability distribution function (PDF). Prior PDF is based on previously published data, pilot studies or the expectations of the experimenter. Based on the PDF, the mode (QUEST) or the mean (ZEST) stimulus intensity that is most likely to be the subject's threshold is presented. The subject's response is then used to construct a new PDF using Bayes' rule of combining probability. The next stimulus intensity is presented at the new level that is most likely threshold. At the end of the procedure, the mode (QUEST) or the mean (ZEST) of the final PDF is considered the best estimate of the subject's threshold.

Spatial resolution, visual acuity and other metrics of visual function

Visual Acuity

Visual acuity is the spatial resolving capacity of the visual system. This may be thought of as the ability of the eye to see fine detail. There are various ways to measure and specify visual acuity, depending on the type of acuity task used. Visual acuity is limited by diffraction, aberrations and photoreceptor density in the eye (Smith and Atchison, 1997). Apart from these limitations, a number of factors also affect visual acuity such as refractive error, illumination, contrast and the location of the retina being stimulated.

Target detection requires only the perception of the presence or absence of an aspect of the stimuli, not the discrimination of target detail (figure 1).

The Landolt C and the Illiterate E are other forms of detection used in visual acuity measurement in the clinic. The task required here is to detect the location of the gap.

Target recognition tasks, which are most commonly used in clinical visual acuity measurements, require the recognition or naming of a target, such as with Snellen letters. Test objects used here are large enough that detection is not a limiting factor, but careful letter choice and chart design are required to ensure that letter recognition tasks are uniform for different letter sizes and chart working distances (Bailey and Lovie, 1976).

Snellen letters are constructed so that the size of the critical detail (stroke width and gap width) subtends 1/5th of the overall height. To specify a person's visual acuity in terms of Snellen notation, a determination is made of the smallest line of letters of the chart that he/she can correctly identify. Visual acuity (VA) in Snellen notation is given by the relation:

$$VA = D'/D$$

where D' is the standard viewing distance (usually 6 metres) and D is the distance at which each letter of this line subtends 5 minutes of arc (each stroke of the letter subtending 1 minute).

The reciprocal of the Snellen Notation equals the angle (in minutes of arc) which the strokes of the letter subtend at the person's eye. This angle is also used to specify visual acuity. It is called the minimum angle of resolution (MAR) and can also be given in log10 form, abbreviated as logMAR.

Some European countries, including Greece, specify their visual acuities in decimal form, which is simply the decimal of the Snellen fraction.

Contrast Sensitivity

Contrast is an important parameter in assessing vision. Visual acuity measurement in the clinic use high contrast, that is, black letters on a white background. In reality, objects and their surroundings are of varying contrast. Therefore, the relationship between visual acuity and contrast allows a more detailed understanding of our visual perception.

Grating patterns are used as a means of measuring the resolving power of the eye because the gratings can be adjusted to any size. The contrast of the grating is the differential intensity threshold of a grating, which is defined as the ratio:

$$C = (L_{max} - L_{min}) / (L_{max} + L_{min})$$

where C can have a value between 0.0 and 1.0; sometimes C is called the modulation, Raleigh or Michelson contrast. The luminance of contrast gratings vary in a sinusoidal manner. This allows the contrast of the grating to be altered without changing the average luminance of the screen displaying the gratings.

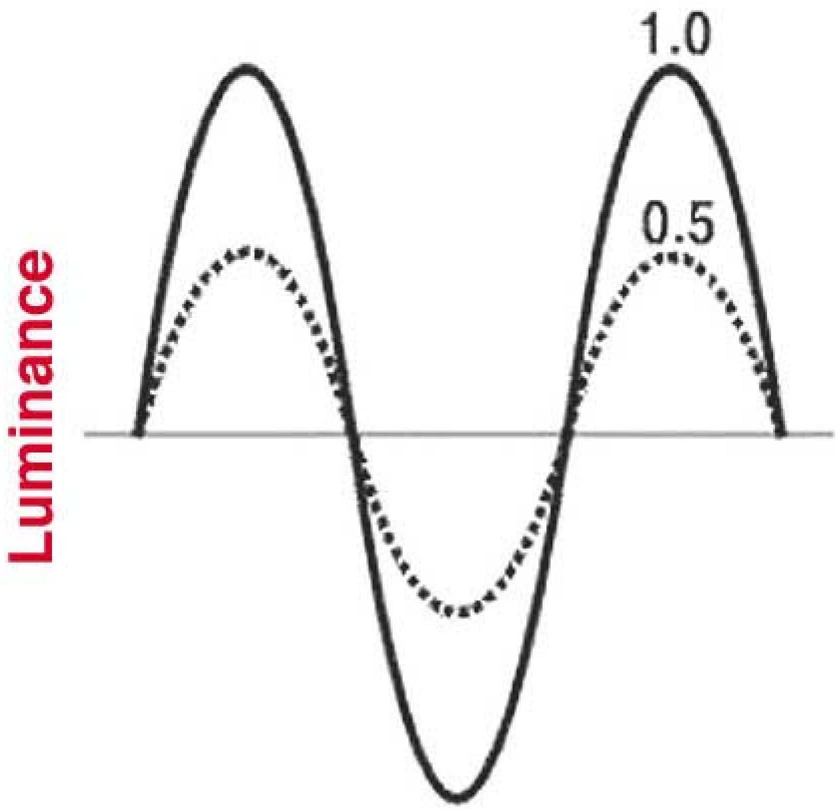

Figure 12: Luminance profile of sinusoidal gratings of contrast ratio of 1.0 and 0.5

Spatial Resolution

The size of the bars of the grating can be expressed in terms of the number of cycles (one cycle consists of one light bar plus one dark bar of the grating) per degree subtended at the eye. This is called the spatial frequency of the grating and can be thought of as a measure of the fineness or coarseness of the grating.

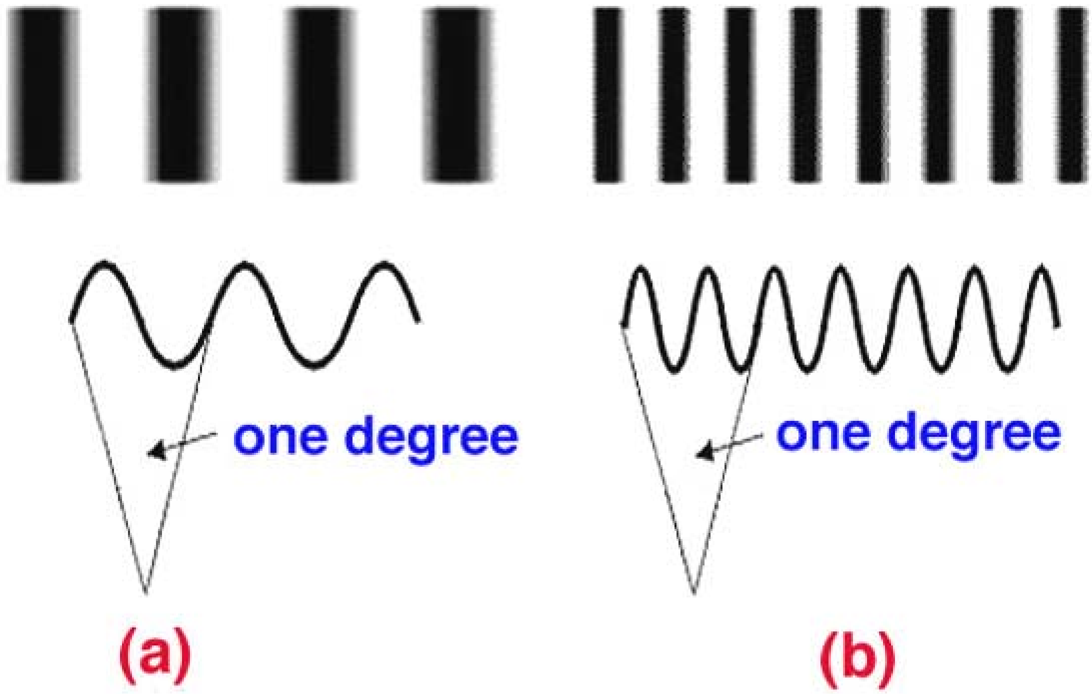

Figure 13: Sinusoidal gratings of different spatial frequencies

Chapter 3: Cone distribution and aliasing

Aliasing

The sampling frequency, at twice the function's Nyquist frequency fc, corresponds for a period function to taking two samples per wavelength. That this is equal to the frequency at which the signals needs to be sampled is obvious in the case of a binary or square grating|resolving it properly requires at least one receptor in the positive and one in the negative portion. Undersampling in the form of taking fewer than two samples per period leads to errors and non-unique reconstructions known as aliasing (falsely translated), a very important phenomenon. In aliasing, the spectra of adjacent copies of ~g(f) overlap with the central copy since $\Delta f < 2fc$. This causes a sine component of frequency f to appear at 2fc - f. C. Since we are here concerned with spatial arrays, we are dealing with spatial aliasing, although everything we have said so far applies equally well to interpolating a temporally discrete function g(t). If temporal aliasing occurs, motion can appear to be reversed, as in the wagon-wheel illusion. Consider an audio-example. The human ear is sensitive to sounds in the 20Hz to 20kHz frequency range. According to the sampling theorem, one should sample sound signals at least at 40kHz in order for the reconstructed sound signal to be acceptable to the human ear. Components higher than 20kHz cannot be detected, but they can still pollute the sampled signal through aliasing. Therefore, frequency components above 20kHz are removed from the sound signal before sampling by a band-pass or low-pass analog filter. Practically speaking, the sampling rate is typically set at 44kHz (rather than 40kHz) in order to avoid signal contamination from the filter that is never perfectly sharp and has a shoulder (also called rolloff).

Depending on the severity of aliasing, we see that the band-limited function g(x) derived from too-coarse sampling contains contributions from high-frequency components of f(x), impersonating low frequencies in a way described by reflection of the high-frequency part around the f = fc axis. This effect can be quite serious as anyone can convince themselves by sampling a sine function of frequency f at intervals greater than 1=2f and gives rise to Moiré patterns as when two window screens or picket fences are superimposed. Once such aliasing has occurred, there is little that can

be done to remove aliased power.

Ideal observer analysis

The ideal observer analysis evaluates the effect of optical stages on the detection of spatial patterns. Human observers not only detect spatial patterns but also are agnostic about the appearance of spatial patterns and, therefore, provide an incomplete evaluation of the impact of optical stages on resolution. For example, the ideal observer analysis revealed that the packing geometry of receptors has little or no impact on ideal contrast sensitivity and that the only effect of varying receptor density is to produce a vertical shift in the ideal CSF. However, it is well known that packing geometry and density can strongly influence the aliasing artifacts that can plague imaging systems. An example of aliasing produced by an electronic still camera can be seen below.

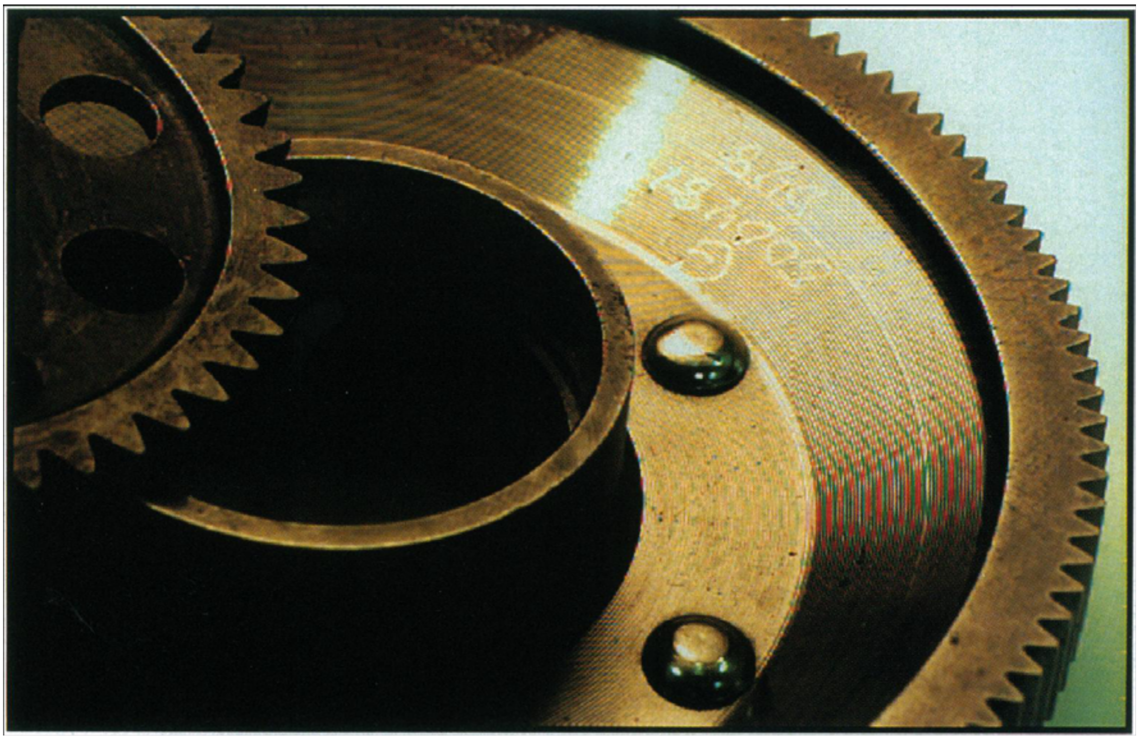

Figure 14: Chromatic aliasing produced by a camera with a three-color CCD (Williams, 1993)

The camera has a trichromatic sampling array not fundamentally different from the human retina; it containes a single charge-coupled device array in which each pixel is covered with one of three colored filters. The image is degraded by a chromatic moiré pattern as well as color distortion where there are highlights. These distortions arise because the spacing of each of the three sampling arrays in the charge-coupled device array is too large to faithfully represent the fine detail in the original scene. There is considerable direct evidence for such sampling limitations in human vision. Williams showed that observers viewing interference fringes with spatial frequencies exceeding the cone Nyquist frequency see coarse wavy patterns that resemble zebra stripes. He showed that these patterns are aliases of the original stimulus produced by the cone mosaic. Brewster described a phenomenon in which fine black and white gratings appear to contain broad splotches of pastel hues.

Williams et al. established that this phenomenon is directly analogous to the chromatic distortions shown above. They found stimulus conditions in which Brewster's colors were produced by chromatic aliasing in the M- and L-cone mosaics. Sekiguchi et al. found additional evidence for aliasing by these submosaics when observing red-green isoluminant interference fringes that exceeded the resolution limit. Williams and Collier found stimulus conditions that produced chromatic aliasing by the S-cone mosaic alone.

Cone distributions

Foveal

Studies of monkey and human retinae have shown that cones that are functional during daylight, photopic, vision form a very regular hexagonal mosaic near the fovea, the point of highest resolution. In the fovea, no rod photoreceptors exists; furthermore, blue sensitive cones appear absent in the central region of the fovea. The packing is dense: adjacent photoreceptors directly touch each other, with an approximate center-to-center spacing of dcc = 3 μm This can be related to the angular spacing between photoreceptors.

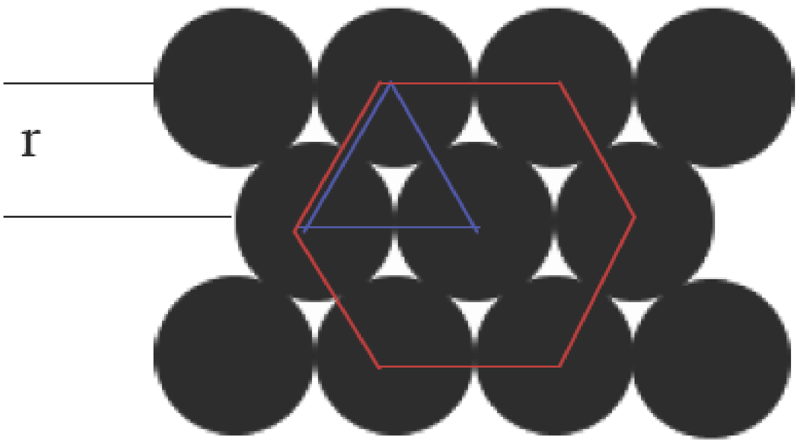

Figure 15: Depiction of hexagonal cone pattern at the fovea

The foveal pattern of cone photoreceptors may be drawn as above. Hoever, it is more realistically depicted in the following figure, along with a superposition of a letter E of about 20/20.

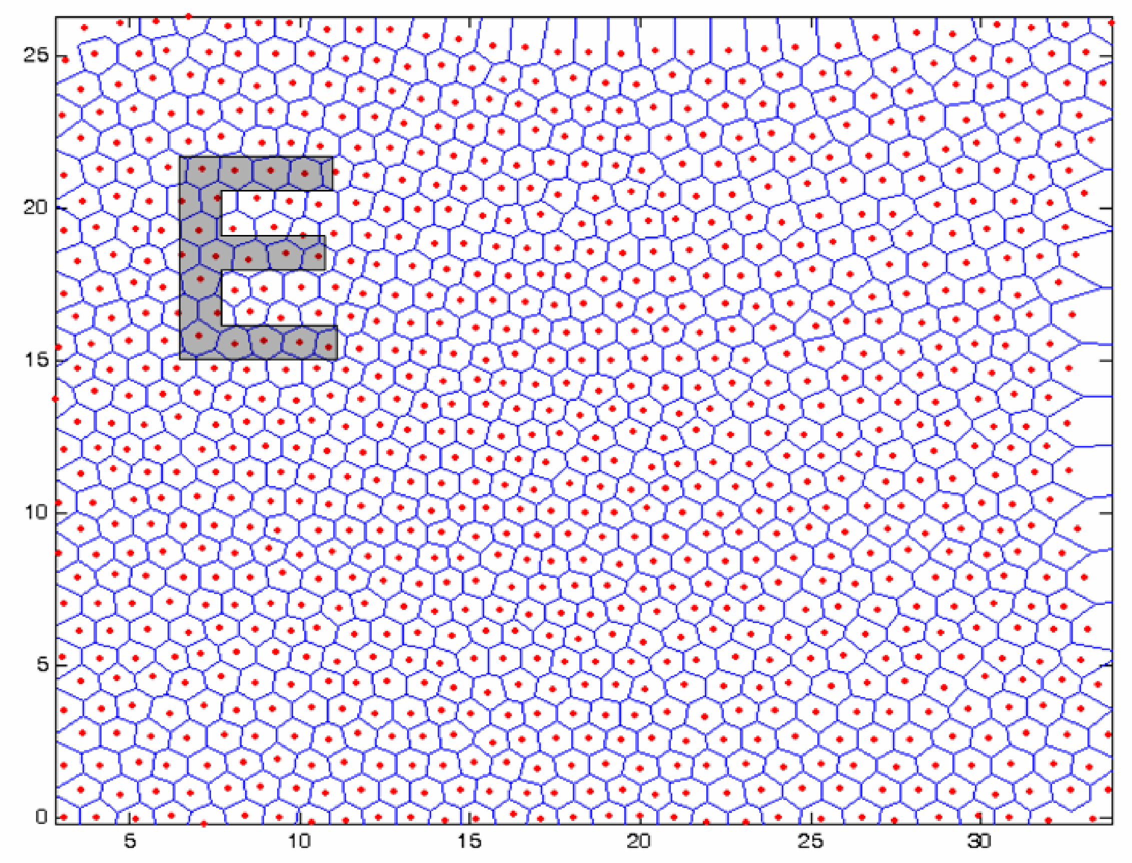

Figure 16: Depiction of quasi-symmetrical cone pattern at the fovea (courtesy H. Ginis)

Departing even more from the random node displacement iquasi-regular pattern, one may even use the following depiction, which is based on identical equilateral pentagons that tile the plane, which may be arranged in a variety of ways. This method may be quite suitable in that the shape of photoreceptors varies only slightly, however no pattern is actually repeated at the individual photoreceptor level, even though small identical groups emerge, depending on the orientation of the tiles.

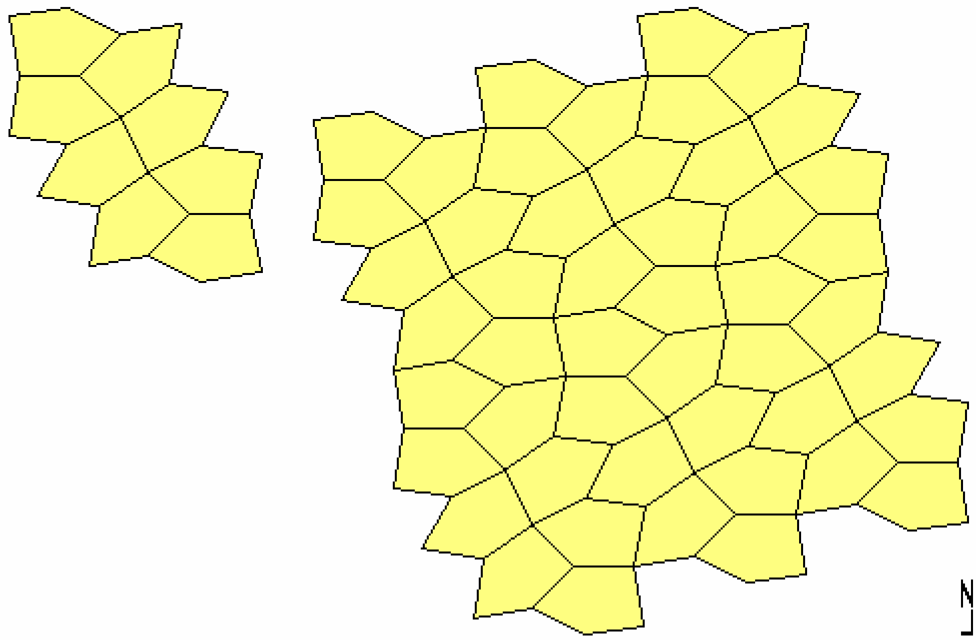

Figure 17: Alternative retina tiling using equilateral pentagons

Parafoveal

What about spatial perception in the extrafoveal region, where the cone sampling rate drops precipitously with increasing retinal eccentricity, while the optical quality declines much more slowly? For instance, at 6° eccentricity the spatial bandwidth of the retinal image is 60 cycle/deg, just as in the fovea, while the Nyquist limit implied by local cone density has fallen from its foveal peak of 60 cycle/deg to 15 cycle/deg (due to intrusion of rods in the spaces between cones). The graph from Hirsch and Miller (1987) shows how the mean $\Delta\varphi$ (or, rather, the associated sampling limit) varies across the retina and compares this function against the pooled human acuity function at different retinal eccentricities as assessed by psychophysics. From the foveal center to about 1.5° of retinal eccentricity, the best-estimate acuity line fits the sampling limits, while at higher eccentricities the system performs worse than predicted from this simple-minded application of signal theory. Yet fine gratings viewed extrafoveally never look like coarse ones. Do neuronal mechanisms somehow prevent aliasing from occurring?

One important fact we have not yet taken into consideration is that the cone receptor packing becomes much more irregular when moving from the fovea to the periphery. The spacing does not become completely random but can be modeled as a Poisson disk distribution: points scattered in the plane according to a Poisson distribution, but subject to the restriction of a fixed minimum distance between each point and its nearest neighbor (in the 1-D case, this is equivalent to a Poisson process with a refractory period).

What will noise do to the sampling process? Papoulis proves in his book that a deterministic function f(t) can be sampled by a Poisson process of mean rate λ without the imposition of a Nyquist frequency (in other words, the sampling does not occur on a regular but on a random lattice, where the sampling points are given by a Poisson process). However, this only works if the sampling frequency λ is high enough or if the sampling interval is large enough so that enough points are sampled. Although Poisson sampling produces no spatial aliasing in the limit, their cost is spectral scattering that a ects high and low spatial frequencies equally, so that the postsampled image is always masked by a veil of white noise.

Yellott (1983) computed optically the Fourier transform of the cone sampling lattice of the parafoveal monkey cone array: the spectrum is a single delta function at zero surrounded by a circular island of empty space whose radius R is on the order of 110 cycles per degrees (the inverse of $\Delta\varphi$). Sampling this array with a sine wave of frequency $f < R=2$ escapes masking by the noise (that is, frequencies lower than the Nyquist frequency for the associated regular array), whereas higher frequencies are scattered into broadband noise, rather than being aliased as low-frequency signals.

As proposed by Yellott (1983), it may well be that evolution uses random receptor sampling to avoid aliasing due to a mismatch between superior optical qualities and a low receptor count. Other mechanisms, such as neuronal pooling of the signal, very likely also prevent aliasing by averaging over the relevant frequency band.

Peripheral

When moving from the parafoveal region to the periphery, the irregularities become more pronounced.

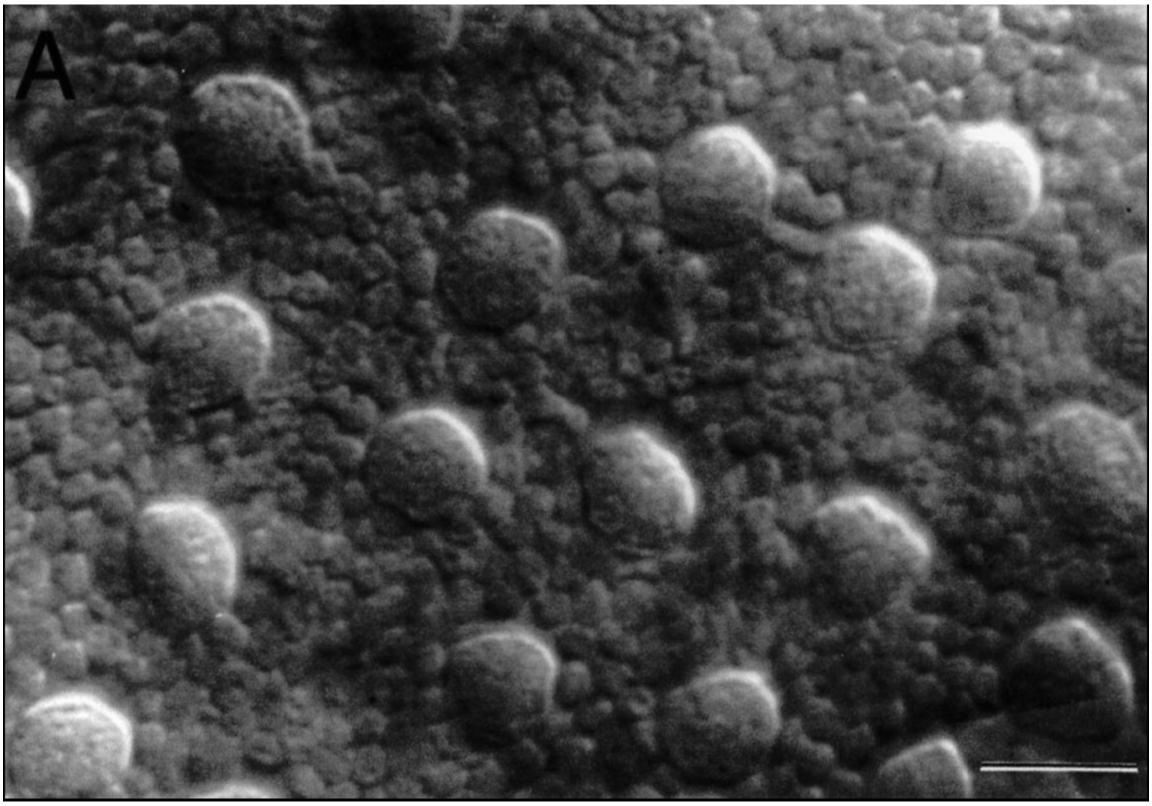

Figure 18: : Photomicrograph of the mid-nasal periphery of the retina (Williams, 2000)

Eventually, the cone mosaic pattern becomes totally random, where now organizational unit of cones may be perceived as being a repeatable element of tiling the retinal plance. This instantly leads to a collapse of all aliasing effects, which only appear if the cone distribution is non-random at least along one axis on the retinal plane.

This collapse is further amplified by the scarcity of neural cells and the great increase in receptive field size, which leads to gross averaging of fine gratings in the periphery.

Chapter 4: Image enhancement and anti-aliasing

Adaptive Optics

Adaptive Optics can be used to either achieve real-time in-vivo imaging of the retinal mosaic (albeit not quite at the foveal pit) or a series of high quality offline images that can be calibrated, registered and post-processed. The latter gave birth to the recent advances in blind deconvolution, which have already been used successfully on astronomical data and simulated vision science data (more on that below).

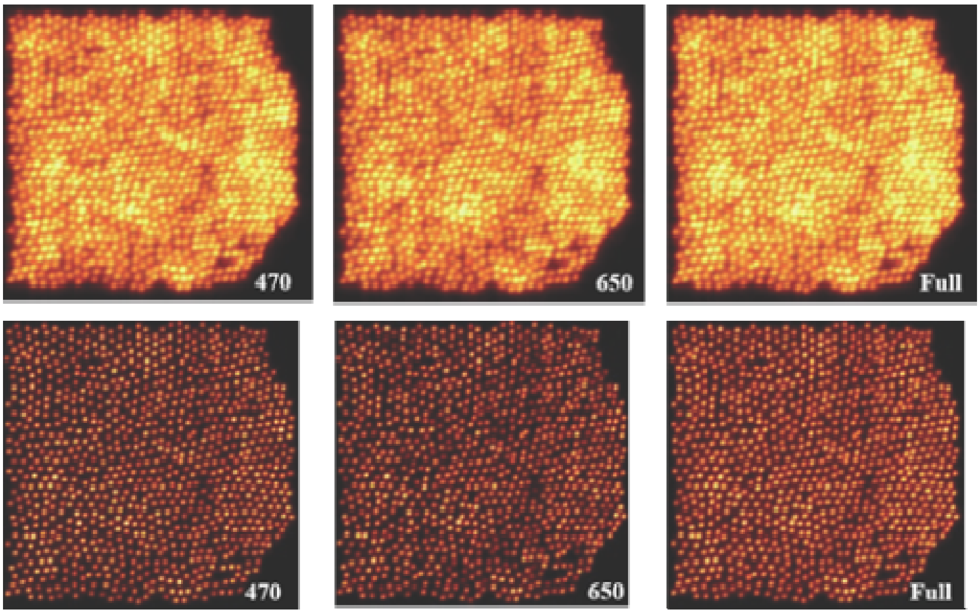

Figure 19: Simulated photoreceptor mosaic as depicted through AO, /w & /wo BD

The quality of real-life images has been steadily increasing in recent years, lately closely resembling the simulated ones. At the same time, AO systems are becoming more affordable and automatic registration algorithms more mature.

Soon, it may be possible to achieve images like the second row of the above figure, with AO and automatic registration.

Blind Deconvolution

However, as mentioned before, blind deconvolution is also a viable post-processing alternative. Blind deconvolution estimates both the object and PSF from a set of observations. It is able to do this by making use of physical constraints which serve to break the symmetry of what appears to be an untractable problem. These constraints include multiple observations of the same object such that there is one common object with each observation having a different PSF, that each PSF is band-limited due to the finite size of the aperture used for the observations and both objectand PSF have to be positive. Prior information about the average structure of the PSF may also be used. Further details about the procedure are given in the addendum.

Addendum

Thesis Presentation

Results of iterative blind deconvolution algorithm in simulated images (Christou, 2000)

Επίδραση της ανομοιομορφίας του πλέγματος των φωτοϋποδοχέων στη διακριτική ικανότητα

Επιμέλεια: Μ. Θεοδωράκης

Εξεταστική Επιτροπή: **Ι. Παλλήκαρης**
Μ. Τσιλιμπάρης
Χ. Γκίνης

ΕΛΛΑΔΑ 2008
ΥΠΟΥΡΓΕΙΟ ΕΘΝΙΚΗΣ ΠΑΙΔΕΙΑΣ ΚΑΙ ΘΡΗΣΚΕΥΜΑΤΩΝ
ΕΙΔΙΚΗ ΥΠΗΡΕΣΙΑ ΔΙΑΧΕΙΡΙΣΗΣ ΕΠΕΑΕΚ
ΕΥΡΩΠΑΪΚΗ ΕΝΩΣΗ
ΣΥΓΧΡΗΜΑΤΟΔΟΤΗΣΗ
ΕΥΡΩΠΑΪΚΟ ΚΟΙΝΩΝΙΚΟ ΤΑΜΕΙΟ
ΕΥΡΩΠΑΪΚΟ ΤΑΜΕΙΟ ΠΕΡΙΦΕΡΕΙΑΚΗΣ ΑΝΑΠΤΥΞΗΣ
Η ΠΑΙΔΕΙΑ ΣΤΗΝ ΚΟΡΥΦΗ
Επιχειρησιακό Πρόγραμμα Εκπαίδευσης και Αρχικής Επαγγελματικής Κατάρτισης

1

ΣΥΝΟΨΗ

I. Ο ανθρώπινος οφθαλμός

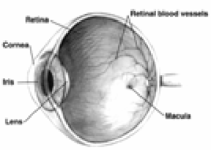

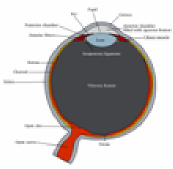

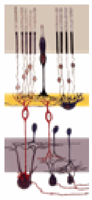

II. Διακριτική Ικανότητα

III. Διάταξη των φωτο-ϋποδοχέων

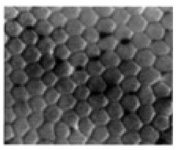

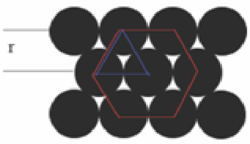

IV. Επίδραση στη διακριτική ικανότητα

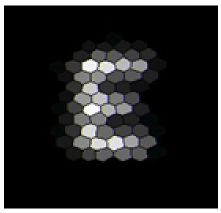

2

Ο ΑΝΘΡΩΠΙΝΟΣ ΟΦΘΑΛΜΟΣ

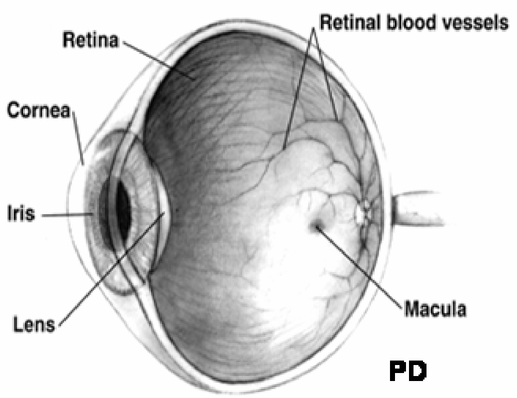

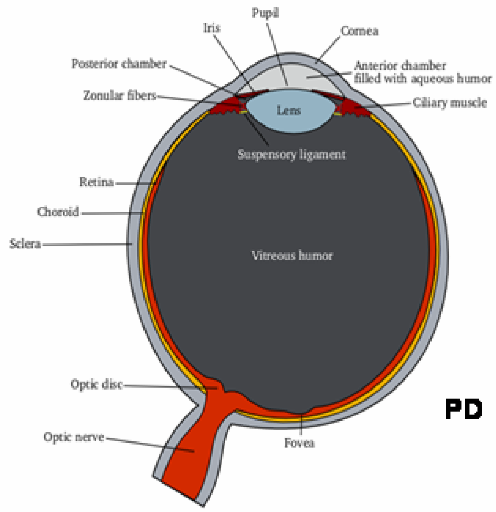

3

Ο ΑΝΘΡΩΠΙΝΟΣ ΟΦΘΑΛΜΟΣ

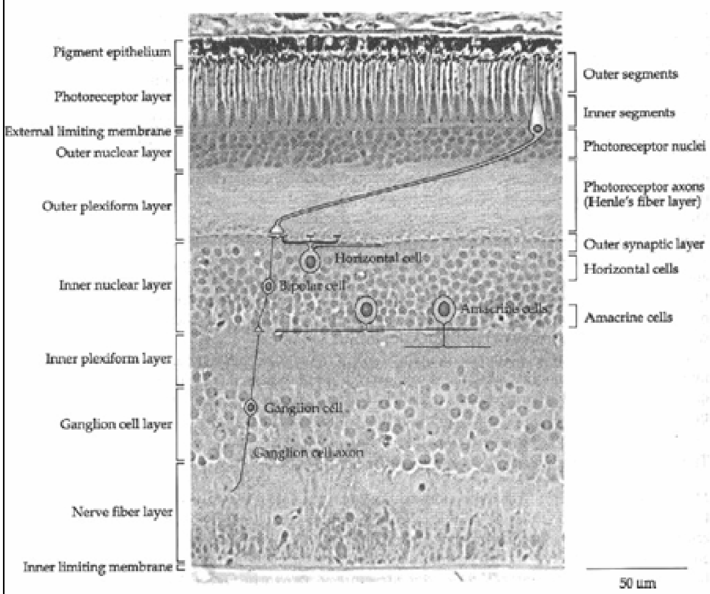

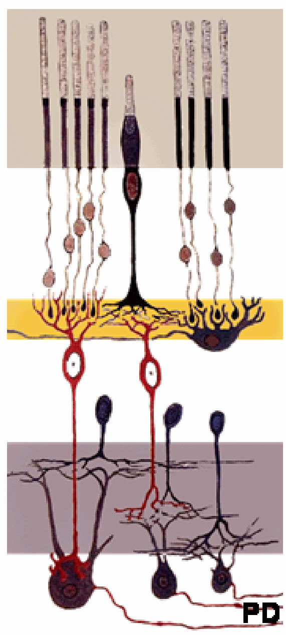

4

Ο ΑΝΘΡΩΠΙΝΟΣ ΟΦΘΑΛΜΟΣ

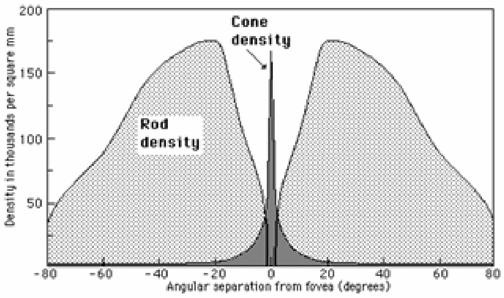

PD, replotted from Oesterberg, 1935

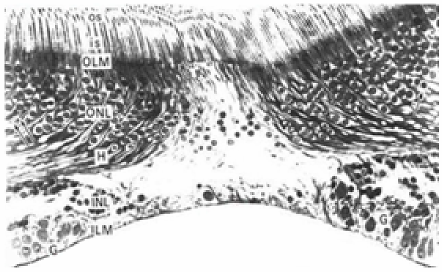

Yamada, 1969

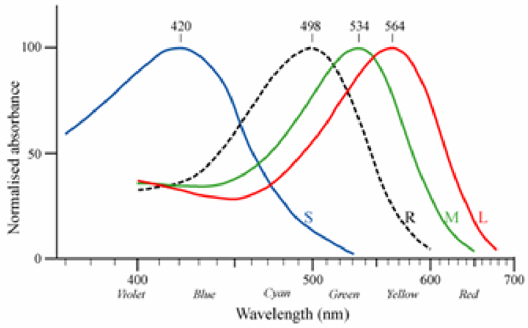

Bowmaker, 1980

5

ΔΙΑΚΡΙΤΙΚΗ ΙΚΑΝΟΤΗΤΑ

- Διακριτική Ικανότητα < Ποιότητα Όρασης
  - Ανίχνευση vs. Αναγνώριση
- Οπτική Συμπεριφορά (Προσεγγίσεις)
  - Ψυχοφυσική (Αρχιμήδης > Helmholtz)
  - Ανατομική
  - Νευροφυσιολογική

<1 c/d

~5 c/d

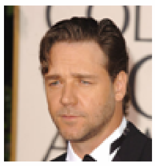

~60 c/d

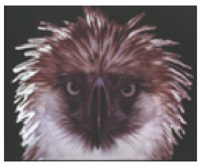

~150 c/d

6

ΔΙΑΤΑΞΗ ΤΩΝ ΦΩΤΟΫΠΟΔΟΧΕΩΝ

excised

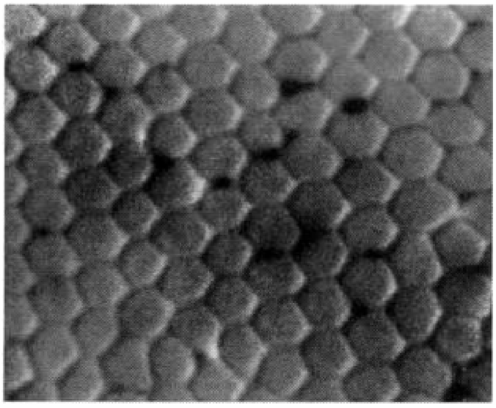

Curcio et al., 1990

in-vivo

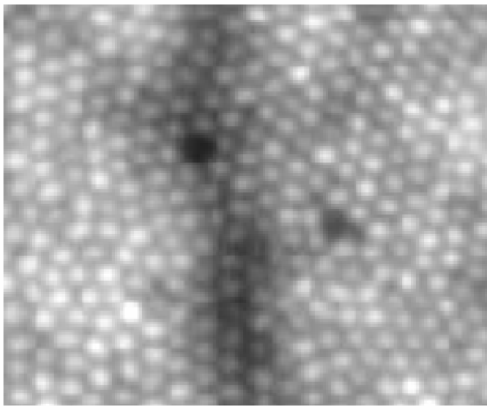

Williams and Roorda, 2001

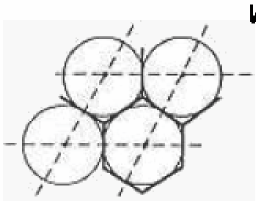

Interlocking hexagons

7

ΔΙΑΤΑΞΗ ΦΩΤΟΫΠΟΔΟΧΕΩΝ

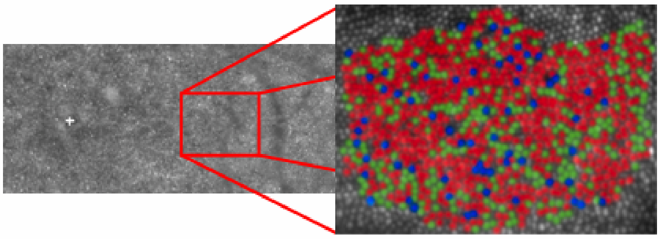

σύνθεση από Williams and Roorda, 2001

$$g_i(r) = f(r) * h_i(r)$$

$$f(r) = ?$$

$$h(r) = ?$$

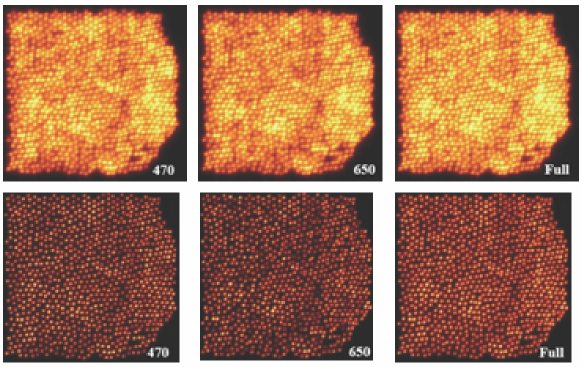

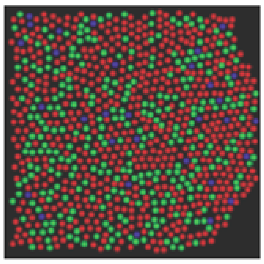

Christou et al., 2004

8

ΔΙΑΤΑΞΗ ΦΩΤΟΫΠΟΔΟΧΕΩΝ

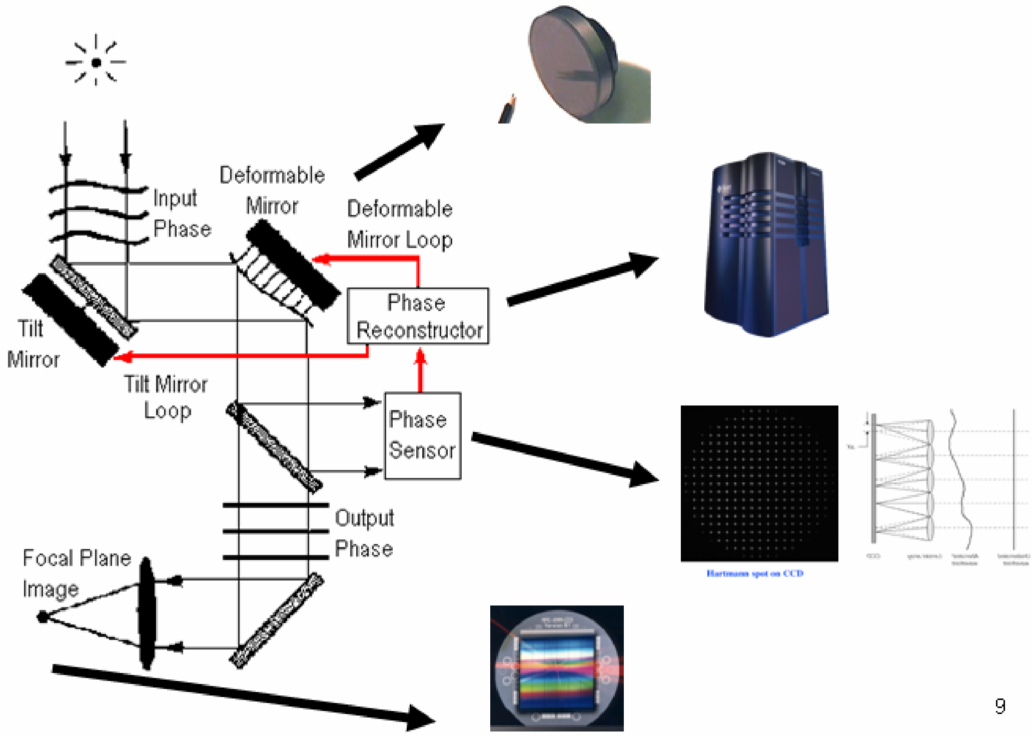

9

ΔΙΑΤΑΞΗ ΦΩΤΟΫΠΟΔΟΧΕΩΝ (ΚΕΝΤΡΙΚΑ)

- In vivo ή in vitro προσδιορίζουμε τη διάταξη του μωσαϊκού (τριγωνική) και την ελάχιστη απόσταση των φωτοϋποδοχέων (~2.5μm στον άνθρωπο)

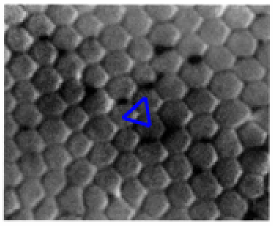

- 120 κωνία / μοίρα
- 60 c/d διακριτική ικανότητα

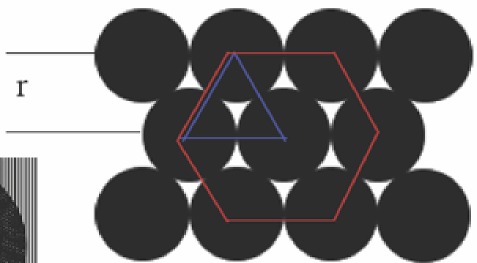

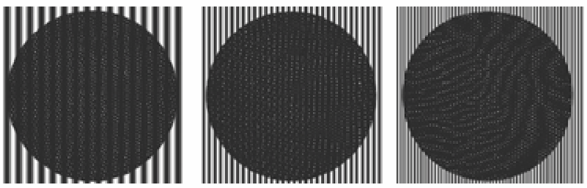

10

ΕΠΙΔΡΑΣΗ ΑΝΟΜΟΙΟΜΟΦΙΑΣ (ΚΕΝΤΡΙΚΑ)

- Στην πράξη, δεν παρατηρείται πάντα aliasing για μεγαλύτερες χωρικές συχνότητες (Koch, 2006).
  - Τα οπτικά του οφθαλμού περιορίζουν τη Δ.Ι. > blur
  - Για μικρές κόρες, επικρατεί η περίθλαση
  - Μεγάλη κόρη, διόρθωση με ΑΟ, εμφανίζεται aliasing πάνω από το όριο (Williams, 2002)

- Απαιτείται η παράλληλη δράση των οφθαλμικών κινήσεων και των ανώτερων επιπέδων επεξεργασίας του οπτικού σήματος.

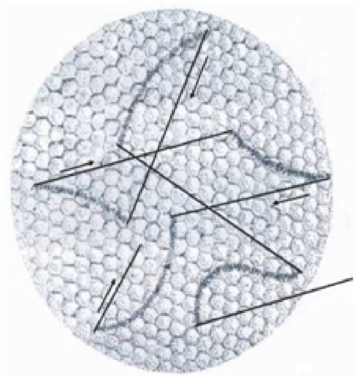

after Pritchard, 1963

ΔΙΑΤΑΞΗ ΦΩΤΟΫΠΟΔΟΧΕΩΝ (ΚΕΝΤΡΙΚΑ+)

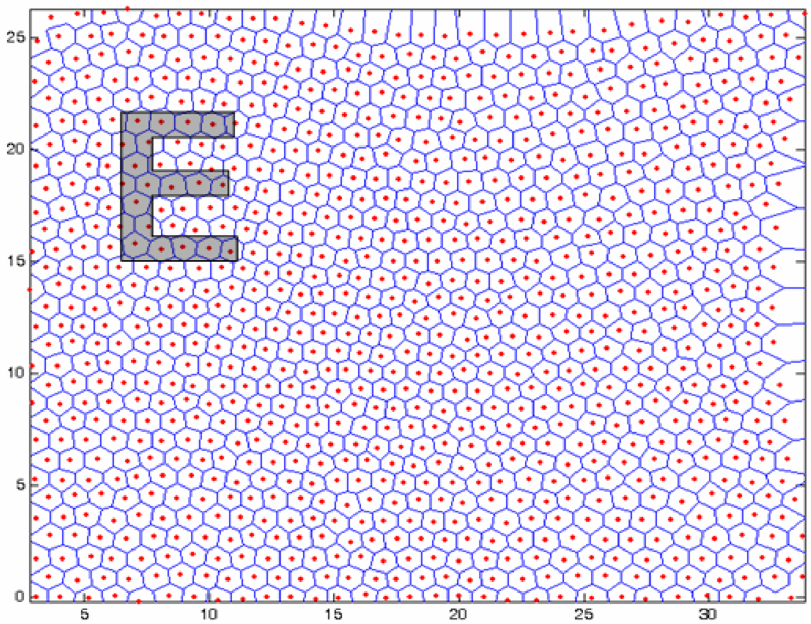

courtesy H. Ginis, A. Pallikaris


ΕΠΙΔΡΑΣΗ ΑΣΥΜΜΕΤΡΙΑΣ
courtesy H. Ginis


ΕΠΙΔΡΑΣΗ ΑΣΥΜΜΕΤΡΙΑΣ
courtesy H. Ginis

ΔΙΑΤΑΞΗ ΦΩΤΟΫΠΟΔΟΧΕΩΝ (ΠΑΡΑΚΕΝΤΡΙΚΑ)

- Μειωμένη πυκνότητα
- Ομοιόμορφη κατανομή
- Εξακολουθούν να παίζουν μεγάλο ρόλο οι οφθαλμικές κινήσεις και τα ανώτερα στάδια επεξεργασίας.
- Όμως, πολύ μειωμένο Nyquist Limit, εξαιτίας της παρεμβολής ραβδίων (~15c/d @ 6°)
- Άρα; Aliasing πέρα από αυτο;
- ΟΧΙ: Μειωμένη συμμετρία > η διάταξη μοντελοποιείται σαν κατανομή Poisson, με τον περιορισμό της σταθερής ελάχιστης απόστασης μεταξύ γειτονικών κωνίων:
- Είναι πολύ πιθανό εξελικτικά να εμφανίστηκε η ψευδο-τυχαία κατανομή για να εξαλειφθεί το aliasing

15

ΔΙΑΤΑΞΗ ΦΩΤΟΫΠΟΔΟΧΕΩΝ (ΠΕΡΙΦΕΡΕΙΑΚΑ)

- Διάσπαρτα κωνία
- Τυχαία κατανομή
- Εξακολουθούν να παίζουν μεγάλο ρόλο οι οφθαλμικές κινήσεις και τα ανώτερα στάδια επεξεργασίας.
- Πάρα πολύ μικρό Nyquist
- Καθόλου aliasing, αλλά και πολύ μειωμένη διακριτική ικανότητα
- Η ασυμμετρία αποτρέπει το aliasing, αλλά η διακριτική ικανότητα δεν ωφελείται σημαντικά από αυτό.

16

ΣΥΜΠΕΡΑΣΜΑΤΑ

- ΚΕΝΤΡΙΚΑ
  - Η Δ.Ι. περιορίζεται από οπτικούς παράγοντες – σχετική ταύτιση ποιότητας οπτικού & νευροφυσιολογικού συστήματος
- ΠΑΡΑΚΕΝΤΡΙΚΑ
  - Η ανομοιομορφία του πλέγματος σε συνδυασμό με τις οφθαλμικές κινήσεις και τα ανώτερα στάδια επεξεργασίας επιτρέπει την αντίληψη και κατανόηση ερεθισμάτων που υπερβαίνουν το Nyquist limit (hyperacuity - Vernier acuity)
- ΠΕΡΙΦΕΡΕΙΑΚΑ
  - Εξαιτίας της πολύ μικρής συγκέντρωσης κωνίων, παρατηρείται μια τυχαία κατανομή, που αποτρέπει τελείως το aliasing. Επιπλέον, διεύρυνση υποδεκτικών πεδίων (μειωμένη γαγγλιακή συγκέντρωση) .Σε συνδυασμό με τις Ο.Κ. ανιχνεύονται σήματα που θα χάνονταν λόγω νευρωνικής υποδειγματοληψίας.

17

ΠΕΙΡΑΜΑΤΑ, ΕΡΕΥΝΑ;

- Άλλες μοντελοποιήσεις του πλέγματος των φωτοϋποδοχέων

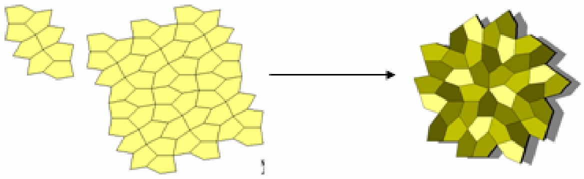

- Βελτιστοποίηση του blind deconvolution για να είναι αποτελεσματικό σε πραγματικά πειράματα (έχει αποτέλεσμα μόνο σε μοντέλα)

- Μελέτη σε φυσικές σκηνές (το power spectrum φαίνεται να αποδίδεται καλύτερα με ασύμμετρο πλέγμα

18

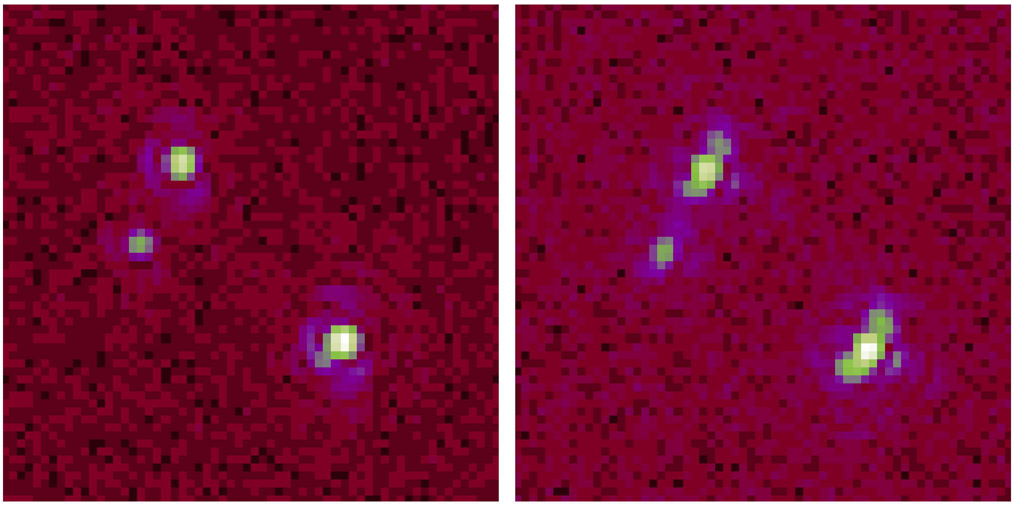

Simulated "observed" data each of which is contaminated by an additive zero-mean Gaussian noise so that the frames have a Signal-to-noise ratio (SNR) (measured from peak signal to rms background) of 400. The above image shows the first two frames of the data set.

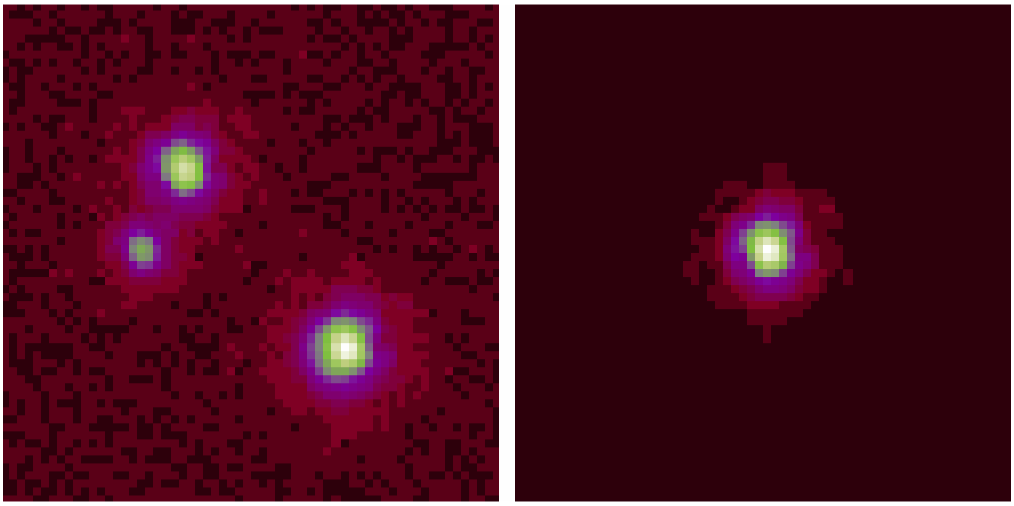

The support files were all set to be unity as was the observation weighting, wt, and the inital object and PSF estimate were set up as the object long exposure and a noise-free long exposure of PSFs (using more than the 10 frames).

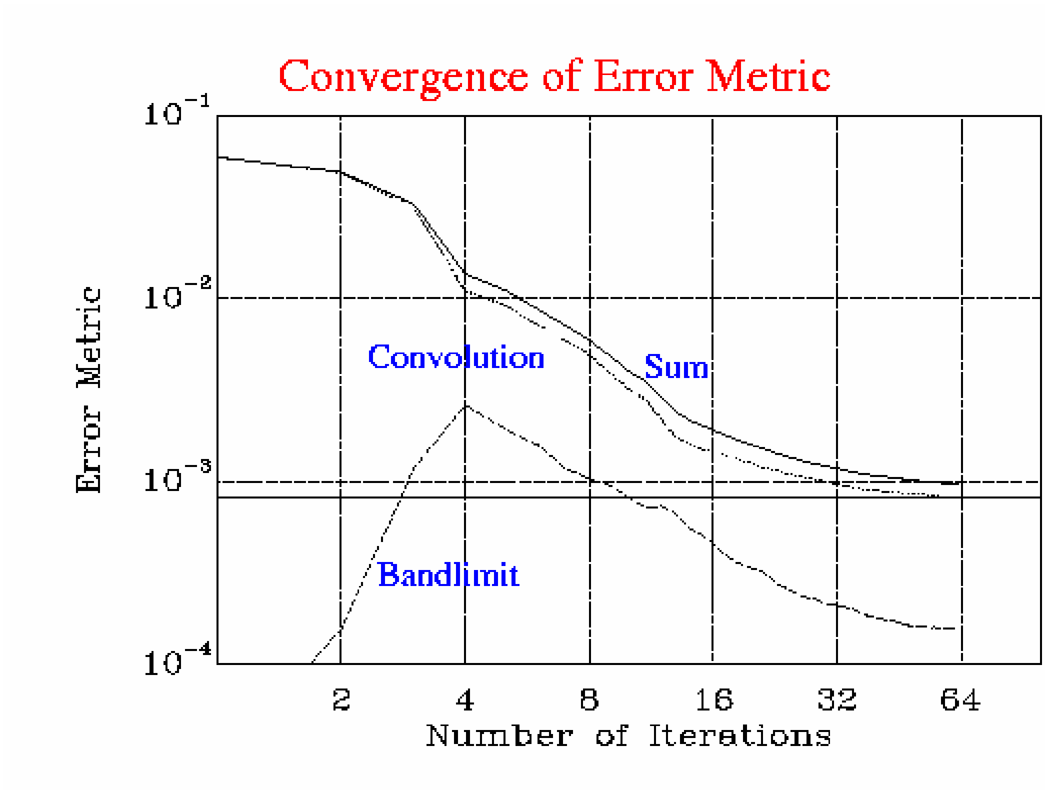

The plot above is a plot of the error metrics for the convergence. Note that for the image domain reduction with no support constraint when E_conv crosses the noise limit then the algorithm has converged.

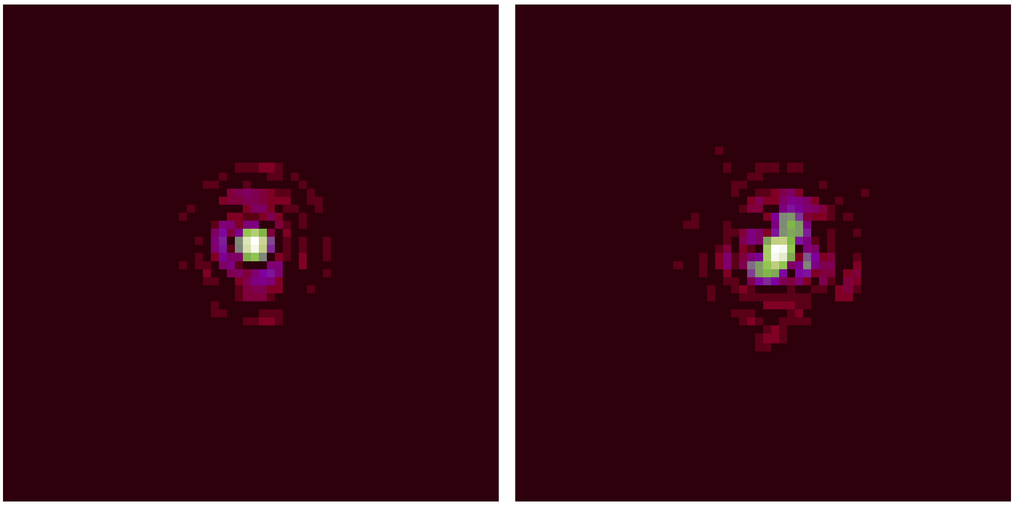

The above images show the recovered PSFs for the first two frames. Compare these to the sample above showing the two distinct morpholgies of the PSFs. Also note the lack of noise in both the the recovered object and PSFs. The PSF's are not registered because the original data was not so that the relative motion of the reconstructed PSF's is the same as for the observations.

References

Books and Articles

Anderson, S. J., N. Drasdo, et al. (1995). "Parvocellular neurons limit motion acuity in human peripheral vision." Proc Biol Sci **261**(1360): 129-38.

Battista, J., M. Kalloniatis, et al. (2005). "Visual function: the problem with eccentricity." Clin Exp Optom **88**(5): 313-21.

Bowmaker, J. K. (1973). "Spectral sensitivity and visual pigment absorbance." Vision Res **13**(4): 783-92.

Bowmaker, J. K. (1981). "Visual pigments and colour vision in man and monkeys." J R Soc Med **74**(5): 348-56.

Bowmaker, J. K. (1983). "How is colour perceived: the visual pigments of human cones." Trans Ophthalmol Soc U K **103 (Pt 4)**: 373-9.

Bowmaker, J. K. and H. J. Dartnall (1980). "Visual pigments of rods and cones in a human retina." J Physiol **298**: 501-11.

Bowmaker, J. K., H. J. Dartnall, et al. (1978). "The visual pigments of rods and cones in the rhesus monkey, Macaca mulatta." J Physiol **274**: 329-48.

Brainard, D. H., A. Roorda, et al. (2000). "Functional consequences of the relative numbers of L and M cones." J Opt Soc Am A Opt Image Sci Vis **17**(3): 607-14.

Calkins, D. J. (2001). "Seeing with S cones." Prog Retin Eye Res **20**(3): 255-87.

Calkins, D. J., S. J. Schein, et al. (1994). "M and L cones in macaque fovea connect to midget ganglion cells by different numbers of excitatory synapses." Nature **371**(6492): 70-2.

Christou, J. C., A. Roorda, et al. (2004). "Deconvolution of adaptive optics retinal images." J Opt Soc Am A Opt Image Sci Vis **21**(8): 1393-401.

Coletta, N. J. and D. R. Williams (1987). "Psychophysical estimate of extrafoveal cone spacing." J Opt Soc Am A **4**(8): 1503-13.

Coletta, N. J., D. R. Williams, et al. (1990). "Consequences of spatial sampling for human motion perception." Vision Res **30**(11): 1631-48.

Curcio, C. A., C. L. Millican, et al. (1993). "Aging of the human photoreceptor mosaic: evidence for selective vulnerability of rods in central retina." Invest Ophthalmol Vis Sci **34**(12): 3278-96.

Curcio, C. A., K. R. Sloan, et al. (1990). "Human photoreceptor topography." J Comp Neurol **292**(4): 497-523.

Doble, N. (2005). "High-resolution, in vivo retinal imaging using adaptive optics and its future role in ophthalmology." Expert Rev Med Devices **2**(2): 205-16.

Geisler, W. S. (1984). "Physical limits of acuity and hyperacuity." J Opt Soc Am A **1**(7): 775-82.

Gowdy, P. D. and C. M. Cicerone (1998). "The spatial arrangement of the L and M cones in the central fovea of the living human eye." Vision Res **38**(17): 2575-89.

Hirsch, J. and C. A. Curcio (1989). "The spatial resolution capacity of human foveal retina." Vision Res **29**(9): 1095-101.

Hirsch, J. and W. H. Miller (1987). "Does cone positional disorder limit resolution?" J Opt Soc Am A **4**(8): 1481-92.

Jacobs, D. S. and C. Blakemore (1988). "Factors limiting the postnatal development of visual acuity in the monkey." Vision Res **28**(8): 947-58.

Jagle, H., E. de Luca, et al. (2005). "Visual acuity and X-linked color blindness." Graefes Arch Clin Exp Ophthalmol: 1-7.

Kimble, T. D. and R. W. Williams (2000). "Structure of the cone photoreceptor mosaic in the retinal periphery of adult humans: analysis as a function of age, sex, and hemifield." Anat Embryol (Berl) **201**(4): 305-16.

Lennie, P. and M. D. Fairchild (1994). "Ganglion cell pathways for rod vision." Vision Res **34**(4): 477-82.

Marcos, S. and S. A. Burns (1999). "Cone spacing and waveguide properties from cone directionality measurements." J Opt Soc Am A Opt Image Sci Vis **16**(5): 995-1004.

Marcos, S. and R. Navarro (1997). "Determination of the foveal cone spacing by ocular speckle interferometry: limiting factors and acuity predictions." J Opt Soc Am A Opt Image Sci Vis **14**(4): 731-40.

Metha, A. B. and P. Lennie (2001). "Transmission of spatial information in S-cone pathways." Vis Neurosci **18**(6): 961-72.

Miller, D. T., D. R. Williams, et al. (1996). "Images of cone photoreceptors in the living human eye." Vision Res **36**(8): 1067-79.

Miller, W. H. and G. D. Bernard (1983). "Averaging over the foveal receptor aperture curtails aliasing." Vision Res **23**(12): 1365-9.

Miyahara, E., J. Pokorny, et al. (1998). "Color vision in two observers with highly biased LWS/MWS cone ratios." Vision Res **38**(4): 601-12.

Mollon, J. D. and J. K. Bowmaker (1992). "The spatial arrangement of cones in the primate fovea." Nature **360**(6405): 677-9.

Pak, M. A. and S. J. Cleveland (1991). "[The spatial frequency limits and the resolving power of the visual system of the pigeon]." EEG EMG Z Elektroenzephalogr Elektromyogr Verwandte Geb **22**(4): 194-9.

Pankhurst, P. M., N. W. Pankhurst, et al. (1993). "Comparison of behavioural and morphological measures of visual acuity during ontogeny in a teleost fish, Forsterygion varium, tripterygiidae (Forster, 1801)." Brain Behav Evol **42**(3): 178-88.

Roorda, A., A. B. Metha, et al. (2001). "Packing arrangement of the three cone classes in primate retina." Vision Res **41**(10-11): 1291-306.

Roorda, A. and D. R. Williams (1999). "The arrangement of the three cone classes in the living human eye." Nature **397**(6719): 520-2.

Roorda, A. and D. R. Williams (2002). "Optical fiber properties of individual human cones." J Vis **2**(5): 404-12.

Siminoff, R. (1991). "Simulated bipolar cells in fovea of human retina. I. Computer simulation." Biol Cybern **64**(6): 497-504.

Thibos, L. N. (1998). "Acuity perimetry and the sampling theory of visual resolution." Optom Vis Sci **75**(6): 399-406.

Troilo, D., H. C. Howland, et al. (1993). "Visual optics and retinal cone topography in the common marmoset (Callithrix jacchus)." Vision Res **33**(10): 1301-10.

Uemura, M., H. Somiya, et al. (2000). "Temporal and mosaic distribution of large ganglion cells in the retina of a daggertooth aulopiform deep-sea fish (Anotopterus pharao)." Philos Trans R Soc Lond B Biol Sci **355**(1401): 1161-6.

Wang, Y. Z., E. Wilson, et al. (2002). "Shape discrimination in age-related macular degeneration." Invest Ophthalmol Vis Sci **43**(6): 2055-62.

Wassle, H., U. Grunert, et al. (1995). "The rod pathway of the macaque monkey retina: identification of AII-amacrine cells with antibodies against calretinin." J Comp Neurol **361**(3): 537-51.

Williams, D., N. Sekiguchi, et al. (1993). "Color, contrast sensitivity, and the cone mosaic." Proc Natl Acad Sci U S A **90**(21): 9770-7.

Williams, D. R. (1985). "Aliasing in human foveal vision." Vision Res **25**(2): 195-205.

Williams, D. R. (1988). "Topography of the foveal cone mosaic in the living human eye." Vision Res **28**(3): 433-54.

Williams, D. R. and N. J. Coletta (1987). "Cone spacing and the visual resolution limit." J Opt Soc Am A **4**(8): 1514-23.

Yellott, J. I., Jr. (1984). "Image sampling properties of photoreceptors: a reply to Miller and Bernard." Vision Res **24**(3): 281-2.

Online Resources

http://webvision.med.utah.edu/index.html (various)

http://en.wikipedia.org/wiki/Main_Page (various)

http://www.geocities.com/liviozuc/pentagons.html

http://www.ics.uci.edu/~eppstein/junkyard/tiling.html

http://www.fortunecity.com/emachines/e11/86/tourist7.html

http://www.nervenet.org/ (various)

http://webexhibits.org/

http://worldcatlibraries.org/ (various)

http://www.optics-vision.gr/ (various)

http://babcock.ucsd.edu/cfao_ucsd/idac/idac_package/idac_index.html